

Evaluation of WRF and CHIMERE models for the simulation of PM_{2.5} in large East African urban conurbations.

Andrea Mazzeo^{1,2}, Michael Burrow¹, Andrew Quinn¹, Eloise A. Marais³, Ajit Singh², David Ng'ang'a⁴, Michael J. Gatari⁴, and Francis D. Pope²

1. School of Civil Engineering, University of Birmingham, Birmingham UK

2. School of Geography Earth and Environmental Sciences – GEES, University of Birmingham, Birmingham UK

3. Department of Geography, University College London, London, UK.

4. Institute of Nuclear Science and Technology, University of Nairobi, Nairobi, Kenya

Correspondence to Andrea Mazzeo (a.mazzeo@bham.ac.uk)

Abstract: Urban conurbations of East Africa are affected by harmful levels of air pollution. The paucity of local air quality networks and the absence of capacity to forecast air quality make difficult to quantify the real level of air pollution in this area. The chemistry-transport model CHIMERE has been used *along* with the meteorological model WRF to run simulations at high spatial resolution of hourly concentrations of Particulate Matter PM_{2.5} for three East African urban conurbations: Addis Ababa in Ethiopia, Nairobi in Kenya, and Kampala in Uganda. Two existing emission inventories were combined to test the performance of CHIMERE as an air quality tool for a target monthly period of 2017 and the results compared against observed data from urban, *roadside*, and rural sites. The results show that the model is able to reproduce hourly and daily temporal variability of aerosol concentrations close to observations in urban, roadside and in rural environments. CHIMERE's performance as a tool for managing air quality was also assessed. The analysis demonstrated that despite the absence of high-resolution data and up-to-date biogenic and anthropogenic emissions, the model was able to reproduce 66 – 99% of the daily PM_{2.5} exceedances above the WHO 24-hour mean PM_{2.5} guideline (25 µg m⁻³) in the three cities. An analysis of the 24-hour average levels of PM_{2.5} was also carried out for 17 constituencies in the vicinity of Nairobi. This showed that 47% of the constituencies in the area exhibited a low air quality index for PM_{2.5} in the unhealthy category for human health exposing between 10,000 to 30,000 people/km² to harmful level of air contamination.

Keywords: Air quality, East Africa, Particulate Matter, Anthropogenic emissions, numerical modelling, Air Quality Index

1 Introduction

The world's population has grown rapidly by 1 billion people in the last 12 years, reaching 7.9 billion in 2021. Future projections suggest a continuing annual increase of 1.8%, meaning the global population will reach 8.5 billion by 2030, 9.7 by 2050, and 11.2 by 2100 (WPP, 2015). The African continent is predicted to have the fastest growing population rate in the world, and it is projected to double between 2010 and 2050, surpassing two billion (WPP, 2011). In addition to this a 60% increase in population has been predicted by 2050, specifically in urban areas (WPP, 2012).

41 Population in Sub-Saharan East African (SSEA) countries have increased drastically ~~from~~ 1991 to 2019. In that
42 period of time and according to data from the World Bank database (WB, 2022), the Kenyan population grew
43 from 24 to 52 million, the Ugandan population from 17 to 44 million and the Ethiopian population from 50 to 112
44 million. These increases in population were accompanied by a similar rate of increase in road transport, industrial
45 activities and in the use of solid fuels (e.g., woods, charcoal, and agricultural residues) for cooking purposes in
46 urban areas (Bockarie et al., 2020;Marais et al., 2019).

Deleted: since

47
48 As a result of these population increases, air quality of the urban areas of these countries, historically influenced
49 by the large presence of seasonal burning biomass emissions (Haywood et al., 2008;Lacaux, 1995;Lioussé et al.,
50 2010;Thompson A. M., 2001), is progressively degrading (Marais and Wiedinmyer, 2016). This, in combination
51 with the expanding urban population, has greatly increased the exposure of citizens to harmful Particulate Matter
52 (PM) pollution with an aerodynamic diameter smaller than 10 and 2.5 μm (PM_{10} and $\text{PM}_{2.5}$, respectively) (Gatari
53 et al., 2019;Kinney et al., 2011;Li et al., 2017;UN-Habitat, 2017).

54
55 Several diseases have been attributed to PM exposure in SSEA, including cardiovascular and cardiopulmonary
56 diseases, cancers, and respiratory deep infections (Dalal et al., 2011;Mbewu, 2006;Parkin et al., 2008). In 2012,
57 the World Health Organization (WHO) estimated that in 2012 176,000 deaths in SSEA were directly connected
58 to air pollution (WHO, 2012). Modelling studies have also found that exposure to outdoor air pollution has led to
59 626,000 disability-adjusted life per year (DALYs) in SSEA alone (Amegah and Agyei-Mensah, 2017),
60 highlighting that these numbers could be much higher considering the limited amount of air quality data emanating
61 from the region that are available for research purposes.

62
63 Considering the likely severe impacts of air pollution on human health in SSEA, the research interest in
64 understanding air pollution trends in East Africa has increased in recent years. Many researchers have analysed
65 the levels of contamination by short-term measurement campaigns (Amegah and Agyei-Mensah, 2017;deSouza
66 P., 2017;Egondi et al., 2013;Gaita et al., 2014;Gatari et al., 2019;Kume, 2010;Ngo et al., 2015;Pope et al.,
67 2018;Schwander et al., 2014;Vliet, 2007;Singh et al., 2021). Other studies observed annual average $\text{PM}_{2.5}$
68 concentrations in the order of $100 \mu\text{g m}^{-3}$ quantified in a small number of urban areas of SSEA (Brauer et al.,
69 2012). These levels are about four times higher than the 24-hour average and ten times higher than the annual
70 average WHO guidelines for $\text{PM}_{2.5}$ (Avis W. and Khaemba W., 2018;WHO, 2016) and underline that air pollution
71 is a serious problem in this area of the world. A recent study by Singh et al. (2020), using visibility as a proxy for
72 PM, showed that air quality in Addis Ababa, Kampala and Nairobi has degraded alarmingly over the last 4
73 decades.

74
75 The lack of long-term air quality monitoring networks in many African countries have made it difficult to have
76 reliable long-term air quality data (Petkova, 2013;Pope et al., 2018;Singh et al., 2020) and still little is known
77 about the levels of air contamination in large urban conurbations (Peña, 2017). The paucity and sometimes
78 complete absence of reliable data on air pollution levels makes it difficult to quantify the magnitude of the
79 problem. Consequently, it is difficult for local and national authorities to plan possible improvement measures for
80 the mitigation of anthropogenic emissions. Even if important steps forward have been made to improve the

82 knowledge relative to anthropogenic emissions and emission inventories for Africa used for numerical simulations
83 and forecasts of air quality (Assamoi and Lioussé, 2010; Lioussé, 2014; Marais and Wiedinmyer, 2016) the lack of
84 surface observations to validate the emission magnitude and the simulated concentrations make these inventories
85 susceptible of large error.

86
87 In this work we test a meteorological and a chemistry-transport model (CTM) to simulate the hourly urban and
88 rural levels of PM_{2.5} in [three SSEA urban conurbations](#) during a monthly period of 2017. We present the results
89 of the validation of both models for the capital cities of Kenya, (Nairobi), Ethiopia (Addis Ababa) and Uganda
90 (Kampala) against observation data. For Nairobi, we compare model outputs with observations from rural and
91 roadside sites observations collected during the “A Systems approach to Air Pollution in East Africa” research
92 project (ASAP-East Africa - www.asap-eastafrica.com, hereafter called ASAP) (Pope et al., 2018). For Addis
93 Ababa and Kampala, the model was validated using hourly observations of PM_{2.5} collected by the respective U.S.
94 Embassies.

95
96 Moreover, we assess the suitability of the CTM as a decision support tool for policy makers to plan possible
97 mitigation policies oriented to quantify the real level of air pollution in urban areas and quantify the human
98 exposure to PM_{2.5}. Specifically, in terms of the accuracy of the model in estimating the daily WHO threshold limit
99 exceedances of PM_{2.5} in the three urban conurbations. Finally, for the particular case of Nairobi, we evaluate the
100 average air quality indices by local constituency for the whole analysed period giving a new insight of the real
101 level of air contamination in Nairobi to the general public and the relative population exposed to harmful level of
102 air contamination.

103 104 2 Material and Methods

105
106 [The meteorological and chemistry-transport models used in this work have been configured to simulate hourly
107 weather parameters and concentrations of PM_{2.5} using available input data for the simulations and observations
108 from the real world for the validation. The availability of the observations for the validation of both models comes
109 from different providers, have different frequency in time and, in the case of PM_{2.5} observations, come from
110 different environments \(rural, urban, roadside sites\). No vertical observations were available for the validation of
111 both models.](#)

112 113 2.1 Meteorological model WRF

114
115 The Weather Research and Forecasting (WRF) model is a numerical model for weather predictions and
116 atmospheric simulations and is used commercially and for research purposes, including by the US National
117 Oceanic and Atmospheric Administration (Powers, 2017; Skamarock, 2008).

118
119 [WRF was used to drive the meteorology for CHIMERE using three geographical domains at different resolutions
120 \(from 18×18 km to 2×2 km\) vertically divided into 30 levels, nine of which are below 1500 m. The first external
121 domain has a spatial resolution of 18×18 km \(Figure 1\), with three nested domains at a resolution of 6×6 km](#)

Deleted: The models have worked on a system of 3 geographical domains at different resolution aimed to run simulation of atmospheric chemistry at 2×2 km of spatial resolution for the first time in this area of the world. ¶

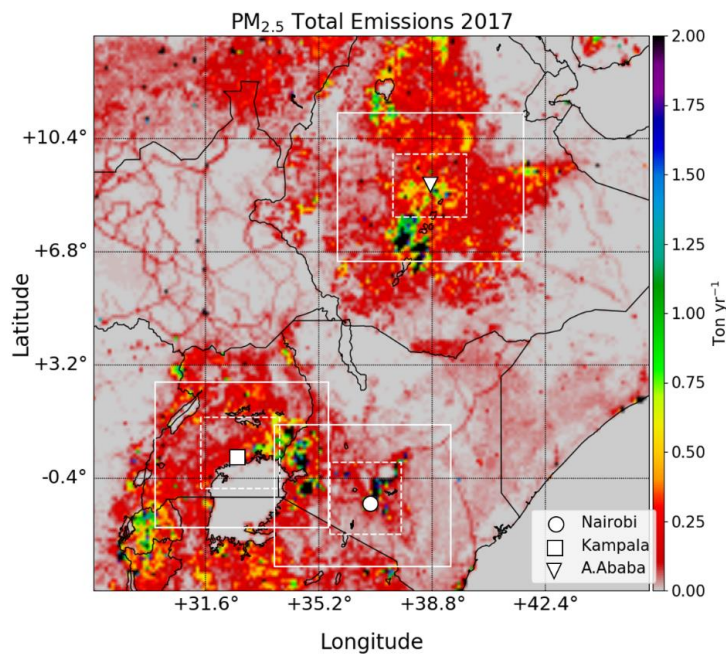
Deleted: s

Deleted: s

129 [centred on the three countries of interest \(Figure 1, white squares\). Three further nested domains with a resolution](#)
130 [of 2×2 km centred on Addis Ababa, Kampala, and Nairobi \(Figure 1, white dashed squares, and Figure 3a, b, c\)](#)
131 [are the focus of the analysis.](#)

132
133 The configuration adopted for the WRF simulations has been chosen according to previous works made on East
134 Africa (Kerandi et al., 2016;Kerandi et al., 2017;Pohl et al., 2011) and is summarized in Table 1. The Yonsei
135 University Scheme (YSU - (Hong S., 2006)) was chosen to represent the Planetary Boundary Layer while the
136 Community Atmosphere Model (CAM - (Collins, 2004)) was used for the long and short-wave radiation scheme.
137 Initial and boundary conditions for the external coarse domain at 18×18 km were obtained from the NCEP FNL
138 (Final) Operational Global Analysis data (Wu, 2002). Boundary condition for the first (6×6 km) and second (2×2
139 km) nest domains were taken from the respective parent domains using the two-way-nesting approach. The
140 process enables the lateral conditions for the internal domains to be calculated from the outputs of the respective
141 parent domains at lower resolution at every time step of the simulation.

142
143 The land use option chosen for the simulations was NOAH (Tewari, 2004) while the WRF Single-moment 3-
144 class Scheme (WSM3) for clouds and ice proposed by Hong S. (2004) was chosen for the reproduction of the
145 microphysical processes in WRF.



146
147 **Figure 1:** Spatial distribution of the PM_{2.5} emissions from DICE-EDGAR merged emission inventory for East Africa for the
148 WRF domain at 18×18 km of resolution. The continuous white lines show the location of the first nested domain at 6×6 km of
149 resolution used in WRF-CHIMERE. The dashed white squares give the locations of the second nested domains at 2×2 km
150 centred on Addis Ababa (Ethiopia, [white triangle](#)), Kampala (Uganda, [white square](#)) and Nairobi (Kenya, [white circle](#)) used
151 for WRF-CHIMERE.

152

153 2.2 The CHIMERE Chemistry Transport model

154

155 CHIMERE, version 2017r4 (Mailler et al., 2017), is a Eulerian numerical model for reproducing three-
156 dimensional gas-phase chemistry and aerosols processes of formation, dispersion, wet and dry deposition over a
157 defined domain with flexible spatial resolutions. CHIMERE has been used for a number of comparative research
158 studies of Ozone and particulate matter PM₁₀ from the continental scale, (Bessagnet et al., 2016; Zyryanov et al.,
159 2012) to the urban scale (van Loon et al., 2007; Vautard et al., 2007; Mazzeo et al., 2018). Furthermore, the model
160 has been used for event analysis, scenario studies (Markakis et al., 2015; Trehela et al., 2019), forecasts, and
161 impact studies of the effects of air pollution on health (Valari and Menut, 2010) and vegetation (Anav et al., 2011).
162 The authors highlight that the version of CHIMERE adopted is the 2017r4, the most recent available at the time
163 when the present work was realized.

164

165 [CHIMERE model has been used to simulate the first nested domains at 6×6 km and the second nested domains at](#)
166 [2×2 km of spatial resolution. The configuration adopted in this work uses initial and boundary conditions from](#)
167 [the global three-dimensional chemistry-transport model \(LMDz-INCA, Hauglustaine et al. \(2004\)\), both for](#)
168 [gaseous pollutants and for aerosols for the most external domain at 6×6 km of resolution while for the most](#)
169 [internal domains at 2×2 km of resolution, the boundary conditions are calculated from model outputs of the parent](#)
170 [domains. The complete chemical mechanism used for all the simulations was SAPRC-07-A \(Carter, 2010\) which](#)
171 [can describe more than 275 reactions of 85 species. SAPRC-07-A is the most recent chemical mechanism](#)
172 [available for CHIMERE version 2017r4.](#)

173

174 Horizontal and vertical diffusion is calculated using the approach suggested by Van Leer (1979) and the
175 thermodynamic equilibrium ISORROPIA model (Nenes, 1998) is used for the particle/gases partitioning of semi-
176 volatile inorganic gases. The model permits calculation of the thermodynamical equilibrium between sulphates,
177 nitrates, ammonium, sodium, chloride and water dependent upon temperature and relative humidity data.

178

179 [Dry and wet deposition is calculated in CHIMERE. The particle dry deposition velocities are calculated as a](#)
180 [function of particle size and density as well as relevant meteorological variables, including deposition processes,](#)
181 [such as, turbulent transfer, Brownian diffusion, impaction, interception, gravitational settling and particle rebound](#)
182 [\(Zhang et al., 2001\). Wet deposition is described modelled using a first-order decay equation as described in](#)
183 [Loosmore and Cederwall \(2004\).](#)

184

185 Radiative transfer processes are accounted in CHIMERE using the Fast-JX model (Wild, 2000; Bian, 2002). Fast-
186 JX is applied also in other models (Voulgarakis, 2009; Real and Sartelet, 2011; Telford et al., 2013). The photolysis
187 rates calculated by Fast-JX model are validated both inside the limits of the boundary layer (Barnard, 2004) and
188 in the free troposphere (Voulgarakis, 2009).

189

190 Secondary organic aerosols (SOAs), including biogenic and anthropogenic precursors, [are](#) modelled in CHIMERE
191 as described by (Pun, 2006). SOAs formation is represented as a single-step oxidation of the precursors,

Deleted:

Deleted: are

Deleted:

195 differentiating hydrophilic by hydrophobic SOAs in the partitioning formulation. Finally, biogenic emissions were
 196 taken in account within CHIMERE using MEGAN model outputs as described by (Guenther, 2006).

197

198 **Table 1:** Main configuration parameters adopted for the modelling system WRF-CHIMERE for all simulations.

| WRFv3.9.1 Configuration | | |
|----------------------------------------|---------------------------|------------------------------------------------|
| Initial and Boundary conditions | GFS FNL- Reanalysis | Wu (2002) |
| PBL Parametrization | YSU | Hong S. (2006) |
| SW/LW Radiation Scheme | CAM | Collins (2004) |
| Land Use | NOAH | Tewari (2004) |
| Micro Physics Scheme | WSM3 | Hong S. (2006) |
| Vertical Levels | | 30 |
| CHIMERE2017r4 Configuration | | |
| Initial and boundary conditions | LMDz-INCA | Hauglustaine et al. (2004) |
| Anthropogenic Emissions | EDGARv3.4.1 + DICE-Africa | Crippa M. (2018); Marais and Wiedinmyer (2016) |
| Biogenic Emissions | MEGAN | Guenther (2006) |
| Gas/Aerosol Partitions | ISORROPIA | Nenes (1998) |
| Secondary Organic Aerosols | 1 | Pun (2006) |
| Radiative Transfer | Fast-JX | Wild (2000); Bian (2002) |
| Chemistry Mechanism | SAPRC-07-A | Carter (2010) |
| Horiz. / Vert. Transport scheme | VanLeer | Van Leer (1979) |
| Vertical Levels | | 30 |

199

200 2.3 Emission Inventories

201

202 [To correctly describe the impact of anthropogenic emissions on urban air quality of Nairobi, Kampala and Addis](#)
 203 [Ababa, industrial and on-grid power generation emissions from the Emissions Database for Global Atmospheric](#)
 204 [Research inventory \(hereafter EDGAR, version 3.4.1\) \(Crippa M., 2018\) were combined with non-industrial,](#)
 205 [prominent combustion sources from the Diffusive and Inefficient Emission inventory for Africa \(hereafter DICE\)](#)
 206 [\(Marais and Wiedinmyer, 2016\).](#)

Deleted: are

207

208 EDGAR is a global inventory developed for year 2012 and DICE is a regional inventory for 2013. DICE includes
 209 important sources in Africa (e.g., motorcycles, kerosene use, open waste burning, and *ad hoc* oil refining, among
 210 others) that are absent or misrepresented in global inventories. Both inventories represent the most up-to-date
 211 anthropogenic emissions available for East Africa at the time of the air quality model was used for this work. Both
 212 inventories have spatial resolution of 0.1×0.1° and provide annual total of anthropogenic emissions for relevant
 213 gases and aerosols.

214

215 On one hand, EDGAR provides emissions data for CO, NO, NO₂, SO₂, NH₃, NMVOCs, BC, OC, PM₁₀ and PM_{2.5}
 216 as an annual total_s divided by the sector according to the IPCC-1996 classification. All human activities with
 217 exception of large-scale biomass burning are included in EDGAR (Crippa M., 2018). On the other hand, DICE
 218 provides emissions from particular diffuse and inefficient combustion emission sources (e.g., road transport,
 219 residential biofuel use, energy production and charcoal production and use) for gaseous pollutants (CO, NO, NO₂,
 220 SO₂, NH₃, NMVOCs) and aerosols (BC, OC). Seasonal biomass burning that is considered a large pollution source
 221 in Africa is included in DICE as comparable emissions of black carbon (BC) and higher emissions of nonmethane

223 volatile organic compounds (NMVOCs). Emissions from DICE were used to provide annual total emissions for
224 particular emission sources considered to be misrepresented or missing in a global inventory such as EDGAR.

225
226 The preparation of the final emission inventory was carried out in two steps. First, DICE and EDGAR inventories
227 were merged, by pollutant and by sector, following the approach suggested by Marais and Wiedinmyer (2016).

228 PM_{2.5} emissions are included in DICE as individual components of organic carbon (OC) and black carbon (BC)
229 but they need to be expressed as lumped PM_{2.5} in CHIMERE. Therefore PM_{2.5} was calculated as the sum of
230 Organic Carbon (OC - originally present in DICE) multiplied for a conversion factor following Pai et al. (2020)
231 to represent Organic Aerosols emissions and summed with Black Carbon (BC – originally present in DICE) as
232 follows:

$$PM_{2.5} = (OC \times c) + BC \quad \text{Eq. (1)}$$

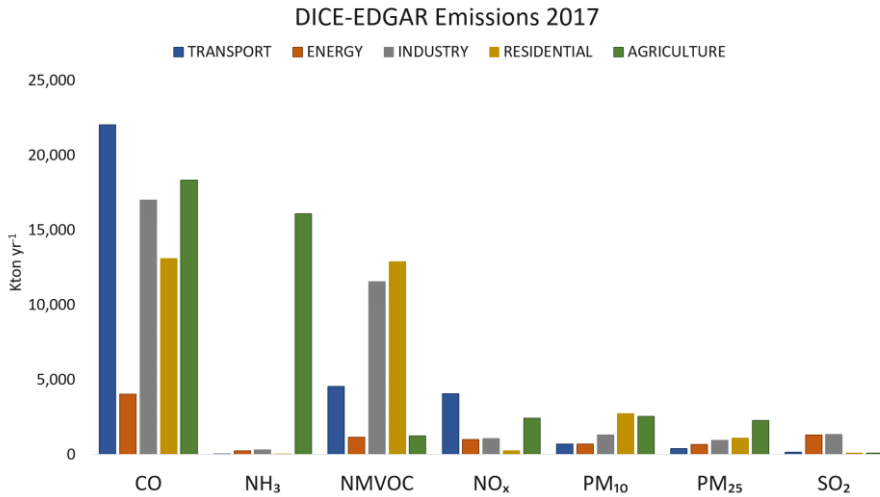
233
234
235
236 Secondly, the emisurf2016 pre-processor of CHIMERE was used to scale the emissions from the original
237 resolution of 0.1×0.1° (~10 km) to the final resolution of each domain simulated (6×6 and 2×2 km) using
238 population density data provided from the Socioeconomic Data and Application Centre (SEDAC)
239 (<http://sedac.ciesin.columbia.edu/>) as proxy for the spatial distribution. SEDAC provides population density maps
240 at high resolution (1×1 km) for the years 2010, 2015 and 2020. The SEDAC population density data calculated
241 for most internal domains at 2×2 km (Figure 3a, b, c) suggest for 2010 a total population of 7 million for Nairobi,
242 4.8 million for Kampala and 4.5 million for Addis Ababa. These totals grow respectively to 8.1, 5.9 and 5.0 million
243 for 2015 and to 9.4, 7.3 and 5.7 million for 2020. The original SEDAC data were used for a linear extrapolation
244 of the population density data to the target year 2017 and were used by emisurf2016 for the spatial allocation of
245 the emissions. [Additionally, emisurf2016 permitted to temporally distribute the original total annual emissions](#)
246 [rates according to seasonal, weekly, and daily variation profiles](#). The resulting merged inventory (hereafter, DICE-
247 EDGAR) totals by pollutant and sectors for the most external domain at 18×18 km of resolution are shown in
248 Figure 2.

249
250 Biogenic emissions and mineral dust considered in this work have been calculated in-line by CHIMERE. The
251 former are calculated by MEGAN model outputs as described by Guenther (2006) while the latter are calculated
252 using the USGS land use database provided by CHIMERE. The soil is represented by relative percentages of sand,
253 silt, and clay for each model cell. The USGS database, called STATSGO-FAO accounts of 19 different soil types
254 recorded in the global database with native resolution of 0.0083×0.0083°. To have homogeneous datasets, the
255 STATSGO-FAO data are re-gridded into the CHIMERE simulation grids. For mineral dust emission calculations,
256 the land use is typically used to provide a desert mask specifying what surface is potentially erodible.

257
258 [The emissions used in this work could still potentially not account for additional misrepresented or unaccounted](#)
259 [sources due to the time difference between the age of the data in the EDGAR and DICE inventories and the](#)
260 [observations used for the validation of the modelling system. The lack of up-to-date national emission inventories](#)
261 [collected at a sufficient resolution, in addition to the lack of research sources providing projections of emissions](#)

Deleted:)

263 [for 2017, meant that it was not possible to generate more detailed information about the anthropogenic sources of](#)
264 [emissions for East Africa.](#)



265 **Figure 2:** Annual Totals for the merged emission inventory DICE-EDGAR for year 2017 calculated on the spatial domain at
266 18×18 km shown in Figure 1.
267

268 It is noted that the time stamp of the anthropogenic emissions and the validation period are different. The emissions
269 are relative to year 2013 while the observation used for the validation for 2017. In the absence of additional data
270 and in the lack of national or local mitigation policies in the three countries we assume that the differences in time
271 stamp do not make large difference to the emission estimates. More detailed analysis of the emission sources and
272 the implementation of possible mitigation policies at national and local levels could in future change this situation.
273

274 Finally, we recall that one of the [main](#) objective of the present work is to evaluate the performance of WRF and
275 CHIMERE models in reproduce meteorology and air pollution levels in urban conurbation_s using the most-up-to-
276 date available data and giving in this way a new insight on the state of the art of the numerical modelling for air
277 quality in this area of the world highlight_{ing} possible improvements for future works.

278 2.4 Weather and Chemistry Observations

279 **2.4 Weather and Chemistry Observations**
280
281 [WRF and CHIMERE models have been validated for a limited monthly period between the 14th of February and](#)
282 [14th of March 2017. The choice of this period is because of the availability of continuous measurements for the](#)
283 [validation of both models. While for the case of WRF observations with frequency variable from 3 to 6 hours are](#)
284 [available from the UK Met Office database for different locations, rarer are PM_{2.5} observations that last over one](#)
285 [month with a measurement frequency of one hour, and from different environments \(rural, urban, or roadside](#)
286 [sites\).](#)
287

288 Moreover, the options chosen for the configuration of the meteorology and chemistry-transport models can result
 289 in better performance in a season more than in another according to the combination of weather and chemical
 290 parameters chosen for both models. The February to March time period in East Africa does not have extreme
 291 temperatures (mean temperatures approximately 10 - 25°C according to the country) and little rainfall that could
 292 affect the observations of weather conditions and PM_{2.5} concentrations (USAID, 2022). These conditions and the
 293 absence of alternative data covering a large time frame for the validation of CHIMERE have constrained the
 294 period of simulation to the present period.

295
 296 **Table 2:** MIDAS ground weather stations used for the validation of the 2×2km domains. Station no. corresponds to the
 297 position of each station in Figure 3a, b and c and PM_{2.5} observation points for the urban domains of Addis Ababa, Kampala
 298 and Nairobi used for the validation of CHIMERE model.

| Station n. | Domain | Name | Lat (°) | Lon (°) | Elev. (m) |
|------------|------------------------------------------------|---------------------------------------------------|---------|---------|-----------|
| 1 | ETH2K | Addis – Bole | 0.03 | 38.75 | 1900 |
| 2 | | Harar Meda | 8.73 | 38.95 | 2355 |
| 3 | | Metehara | 8.87 | 39.90 | 930 |
| | | US Embassy (PM _{2.5} – urban background) | 9.05 | 38.76 | 1900 |
| 4 | UGA2K | Entebbe (Airport) | 0.05 | 32.45 | 1155 |
| 5 | | Kampala | 0.32 | 32.62 | 1144 |
| 6 | | Jinja | 0.45 | 33.18 | 1175 |
| | | US Embassy (PM _{2.5} – urban background) | 0.30 | 32.59 | 1150 |
| 7 | KEN2K | Nairobi (Airport) | -1.32 | 36.92 | 1624 |
| 8 | | Embu | -0.50 | 37.45 | 1493 |
| 9 | | Nakuru | -0.27 | 36.10 | 1901 |
| 10 | | Nyeri | -0.50 | 36.97 | 1759 |
| 11 | | Narok | -1.13 | 35.83 | 2104 |
| | | Tom Mboya Street (PM _{2.5} – roadside) | -1.28 | 36.82 | 1795 |
| | Nanyuki (PM _{2.5} – rural background) | 0.01 | 37.07 | 1947 | |

299
 300 Observations of temperature, wind speed and directions used for the validation of WRF were taken from the UK
 301 Met Office MIDAS database (UK, 2012). Data from 11 weather stations, three for the domain of Ethiopia
 302 (hereafter ETH2K, Figure 3a) and Uganda (hereafter UGA2K, Figure 3b) and five for the domain of Kenya
 303 (hereafter KEN2K, Figure, 3c) were used to validate the simulations at a resolution of 2×2 km (Table 2).

304
 305 The ground stations are at different altitudes above sea level to a maximum of 2355 m (e.g., the Harar Meda
 306 station in Ethiopia, n2 in Figure 3a). The validation was performed by comparing model outputs with observations
 307 for the variables, namely surface temperature, wind speed and direction and relative humidity. The latter, not
 308 originally available in the MIDAS dataset, was calculated using the coefficients proposed by Alduchov O. (1996)
 309 based on hourly surface and dew point temperatures observed values and then compared with modelled data
 310 obtained by WRF.

311
 312 Hourly concentrations of PM_{2.5} were used for the validation of CHIMERE for the three internal domains at 2×2
 313 km (Figure 3a, b, c). For the city of Nairobi, data from roadside background site located at Tom Mboya Street
 314 was used (1.28° S, 36.82° E), while data from the rural background were provided by a site located in Nanyuki,
 315 Kenya (0.01° N, 37.07° E). Both the field sites data were obtained from the field sampling campaign performed
 316 by Pope et al., (2018). For the urban background locations of Addis Ababa and Kampala, hourly concentration of

Deleted: .

Deleted: were provided by the

Deleted: in Nairobi

Deleted:

Deleted:

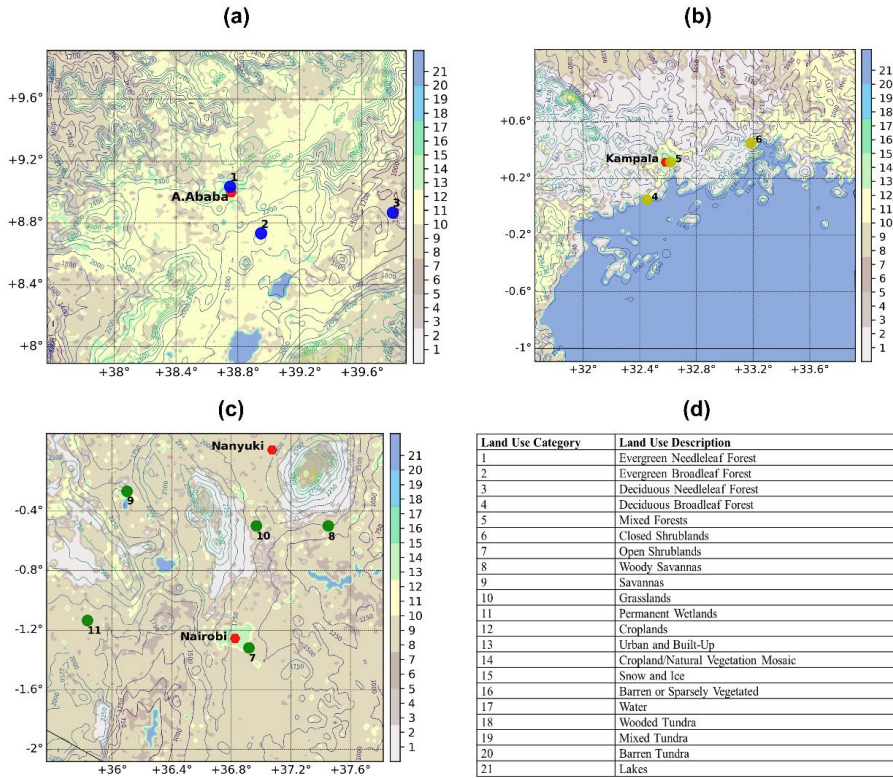
Deleted: the

Deleted: of

Deleted: b

325 [PM_{2.5}](#) were obtained from the air quality monitoring stations of the two U.S. Embassies in Ethiopia (9.05° N,
 326 38.76° E) and Uganda (0.30°N, 32.59° E) using optical counters. Data from Uganda and Ethiopia were used to
 327 compare the configuration applied to CHIMERE for Kenya with the two other countries (Table 2).
 328

Deleted:
 Deleted:
 Deleted:
 Deleted:



329 **Figure 3:** Second-nested domains at a spatial resolution of 2x2 km centred on the cities of Addis Ababa (ETH2K - a), Kampala
 330 (UGA2K - b), Nanyuki and Nairobi (KEN2K - c) created using the WRF model outputs. The red dots represent locations of
 331 [PM_{2.5}](#) measurements. The blue, yellow, and green dots refer to the location of the ground weather stations used for the
 332 meteorological validation in Ethiopia, Uganda, and Kenya, respectively. The numbers relate to the stations detailed in Table
 333 2. Contour lines are relative to the height meters from the ground levels from WRF outputs while the colour scale applied to
 334 the maps a, b and c represents the 21 classes of classification of the land use adopted in WRF simulations. The description of
 335 each land use category is provided in table d.
 336

337 3 Results and Discussion

338 The reliability of numerical simulation of meteorology and chemistry-transport processes need to be evaluated
 339 against observations from the real world to quantify the confidence of these systems. In the case of CTM in
 340 particular, this applies also to the capability to be used as tool for policy making, replicating scenarios and analysis
 341 purposes. While ozone modelling and evaluation has been fairly well developed over a number of decades, with
 342
 343

348 the EPA (1991) criteria still used to evaluate the level of confidence of a CTM, for the PM evaluation the criteria
349 used for the analysis of the performance are still evolving (Boylan and Russell, 2006).

350

351 In this work we use different statistical operators to evaluate the performance of WRF and CHIMERE models in
352 reproducing the main surface weather parameters and hourly and daily concentrations of PM_{2.5} in different urban
353 and rural environments. The statistical parameters of Pearson's Coefficient (R), index of agreement (IOA), mean
354 fractional bias (MFB) and mean fractional error (MFE) have been used for the calculations.

Deleted: and

355

356 MFB and MFE in particular, are metrics specifically used for the evaluation of numerical system for atmospheric
357 chemistry and meteorology. They normalise the bias and the error for each model-observed pair by the average
358 of the model and observation before taking the final average (Eq. 2 and 3). The advantage of these metrics is that
359 the maximum bias and errors are bounded, and that impact of outlier data points are minimised. Moreover, the
360 metrics are symmetric giving equal weight, to concentrations simulated higher than observations and to those that
361 are simulated lower than observations.

$$362 \quad MFB = \frac{1}{N} \sum_{i=1}^N (C_m - C_o) / ((C_o + C_m) / 2) \quad \text{Eq. (2)}$$

363

$$364 \quad MFE = \frac{1}{N} \sum_{i=1}^N |C_m - C_o| / ((C_o + C_m) / 2) \quad \text{Eq. (3)}$$

365

366 MFB and MFE have been expressed in terms of model performance "goals" and model performance "criteria"
367 values according to the methodology proposed by Boylan and Russell (2006). The performance "goal" for the
368 modelling system is attested for $MFE \leq 50\%$ and $MFB \leq \pm 30\%$. In this range of values (shown as green dashed
369 lines in Figure 6) the performance of the model in reproducing the correct magnitude of the concentrations can be
370 considered good. A second larger range of values, called "criteria", is attributed for $MFE \leq 75\%$ and $MFB \leq \pm$
371 60% . Values inside this are (shown as red dashed lines in Figure 6) corresponds to an average model performance.
372 Finally, values with $MFE > 75\%$ and $-60\% > MFB > +60\%$ correspond to a poor representation by the model
373 (labelled "out" in Table 5).

374

375 WRF and CHIMERE models run at spatial resolutions of 18×18, 6×6 and 2×2 km for meteorology and at 6×6 and
376 2×2 km for chemistry for the three domains of East Africa. The statistical analysis shown in the following sections
377 though, describes the validation results for the three internal domains at a resolution of 2×2 km as these are the
378 focus of the present work.

379

380 Ground weather stations from the MIDAS database, included in the 2×2 km domains of all countries, were
381 analysed individually, and shown as average of all stations. The time series and wind roses are relative to the
382 closest stations from MIDAS database to each urban city centre of the three capital cities, namely Addis- Bole
383 (n1 in Table 2), Kampala (n5 in Table 2) and Nairobi Airport (n7 in Table 2).

384

385 Initially, the performance of CHIMERE was analysed for the domain of Kenya for which hourly concentrations
386 of PM_{2.5} were taken from two different sites (roadside and rural) from the field sampling campaign described by
387 Pope et al., (2018). Secondly, the same configuration adopted for Kenya was used for Ethiopia and Uganda to test

389 both the homogeneity of the emission rates on other urban conditions, and the configuration chosen for CHIMERE
390 in different urban and environmental conditions. At this stage of the validation, a threshold limit of 25 $\mu\text{g m}^{-3}$ for
391 $\text{PM}_{2.5}$ per day provided by WHO (WHO, 2005) was used to quantify the number of exceedances observed and
392 modelled by CHIMERE for the three cities.

393
394 [The validation process was hindered by the highly variable quantity and quality of available meteorological data.](#)
395 [The majority of the weather observations are provided on a 3-hourly basis, with varying amounts of missing data.](#)
396 [Despite this, the statistical evaluation of WRF has been performed comparing model and observations only when](#)
397 [the latter were available. We recall that the objective of this work aims to test the performances of a modelling](#)
398 [system for the simulation of air quality at high resolution for East Africa, updating and/or using the available input](#)
399 [data available and assessing the possible adoption of these tools for air quality policy making at this extent of the](#)
400 [data.](#)

Deleted: for

401

402 3.1 Validation of the WRF simulations

403

404 In order to assess the performance of WRF in simulating surface temperature, relative humidity wind speed and
405 direction, the model simulation outputs were compared with all the available ground weather station data available
406 for the period of analysis, 14th of February to 14th of March 2017. Observations from the UK Met Office MIDAS
407 database were available with variable frequency ranging from 1 to 6 hours.

408

409 3.1.1 Statistical evaluation of WRF performances

410

411 [A statistical analysis, in terms of the mean fractional bias \(MFB\), mean fractional error \(MFE\), index of agreement](#)
412 [\(IOA\) and Pearson's coefficient \(R\), was carried out to compare modelled and observed values for the domain at](#)
413 [2x2 km resolution averaging the observed and modelled values on all the stations present on each domain \(Table](#)
414 [3\). We recall that the number and location of the stations is variable between the three domains \(3 stations for](#)
415 [ETH2K and UGA2K and 5 stations for KEN2K\).](#)

416

417 [The results of the statistical analysis show that WRF is capable of reproducing the mean levels of surface](#)
418 [temperature better for the domain of Ethiopia \(ETH2K\) and Uganda \(UGA2K\) with a mean underestimation over](#)
419 [the three domains of 1.4 and 1.5 °C, respectively, then for Kenya \(KEN2K\) where it shows an underestimation of](#)
420 [4.1 °C. The higher bias in surface temperature found on the average of all five stations of Kenya is though highly](#)
421 [driven by a particular poor representation of this variable at the observation point of Narok \(n11 in Figure 3c\)](#)
422 [where the bias between model and observations is 10.9 °C. A reason for this bias can be related by the location of](#)
423 [the station that is the one at highest altitude of all the Kenyan weather stations \(2104 m a.g.l.\). Narok is located](#)
424 [around 140 km west from Nairobi and the high bias in temperature should not have any effect on the levels of](#)
425 [temperature modelled in the capital of Kenya were the bias for the individual station of Nairobi \(n7 in Figure 3c\)](#)
426 [found was 1.3 °C.](#)

427

429 Relative humidity is overestimated by WRF in KEN2K of 0.2 % and underestimated in ETH2K of 6.4 % and in
 430 UGA2K of 7.5 % (Table 3). Wind Speed and directions for the three domains show respectively, the presence of
 431 northern winds in UGA2K correctly captured by the model with a difference of around 4° in comparison with the
 432 observations, an average eastern wind component in KEN2K partially reproduced by the model that allocates the
 433 average wind directions on a more south-eastern component of wind with a difference of around 40.2° while in
 434 ETH2K the average wind direction modelled and observed are closer with a difference of 4.2° on a south-eastern
 435 component of prevailing wind. The observed and modelled wind speeds in UGA2K, KEN2K and ETH2K are in
 436 reasonable agreement with a model overestimation of 0.9, 0.8 and 0.2 m s⁻¹, respectively (Table 3).
 437

438 **Table 3:** Statistical analysis of relative humidity, surface temperature, wind speed and directions averaged on all the available
 439 weather stations for the second nested domains UGA2K, KEN2K and ETH2K at 2×2 km of resolution. Mean observed and
 440 modelled values (Obs. Mean, Model Mean), Pearson's Coefficient (R), index of agreement (IOA), mean fractional bias (MFB)
 441 and error (MFE) have been calculated.

| | Rel. Humidity (%) | | | Temperature (°C) | | |
|-------------------|--------------------|--------|--------|---------------------------------|--------|-------|
| | UGA2K | KEN2K | ETH2K | UGA2K | KEN2K | ETH2K |
| Obs. Mean | 68.2 | 63.1 | 51.3 | 24.5 | 23.2 | 22.7 |
| Model Mean | 60.7 | 63.3 | 44.9 | 23.0 | 19.1 | 21.3 |
| MFB | -21.52 | -21.36 | -33.02 | 0.17 | -24.25 | -5.38 |
| MFE | 30.08 | 32.25 | 35.56 | 12.50 | 27.94 | 11.34 |
| IOA | 0.44 | 0.44 | 0.47 | 0.43 | 0.31 | 0.53 |
| R | 0.3 | 0.4 | 0.7 | 0.3 | 0.5 | 0.6 |
| | Wind Dir (degrees) | | | Wind Speed (m s ⁻¹) | | |
| | UGA2K | KEN2K | ETH2K | UGA2K | KEN2K | ETH2K |
| Obs. Mean | 6.8 | 91.5 | 104.0 | 2.5 | 2.7 | 3.5 |
| Model Mean | 2.8 | 131.7 | 99.8 | 3.4 | 3.5 | 3.7 |
| MFB | 32.02 | -30.57 | -9.94 | 91.25 | 36.83 | 18.89 |
| MFE | 62.01 | 70.55 | 60.18 | 94.59 | 54.35 | 50.63 |
| IOA | 0.39 | 0.40 | 0.46 | 0.26 | 0.41 | 0.31 |
| R | 0.3 | 0.2 | 0.2 | 0.1 | 0.5 | 0.4 |

Deleted: 67

Deleted: 49

442
 443 All the relative humidity and surface temperature values of MFE were found in the performance goal range for
 444 the three domains: UGA2K (30.08 and 12.50, respectively) KEN2K (32.25 and 27.94) and ETH2K (35.56 and
 445 11.34). The same evaluation done on wind direction and speed shows for the former MFE values inside the criteria
 446 performance range (62.01 for UGA2K, 70.55 for KEN2K and 60.18 for ETH2K) but for wind speed only KEN2K
 447 and ETH2K are in the criteria range (54.35 and 50.63, respectively) while wind speed in UGA2K is found outside
 448 the range of acceptability of the metric (94.59) (Table 3). The MFB analysis shows that surface temperature is
 449 inside the range of performance goal in all three domains with UGA2K (0.17) showing the best performance in
 450 reproducing the variable followed by ETH2K (-5.38) and KEN2K (-24.25). The MFB values inside the goal
 451 criteria were found for the domain of UGA2K and KEN2K also for relative humidity (-21.52 and -21.36) while
 452 for ETH2K the value of MFB was found in the criteria range (-33.02). The ETH2K is the only domain that shows
 453 MFB in the goal range for the evaluation of wind direction (-9.94) and speed (18.89). The domain of Kenya
 454 (KEN2K) shows both values inside the criteria range with -30.57 for wind direction and 36.83 for wind speed.
 455 Finally, UGA2K shows wind direction inside the criteria range (32.02) but wind speed outside the range of
 456 acceptability of this metric (91.25) (Table 3).

459
460 The calculated Pearson's coefficient (R) shows varying agreement between the model and observations [with](#)
461 [values](#) between 0.1 and 0.7 for the three domains. The highest R value for relative humidity of approximately 0.7
462 was obtained for ETH2K while the lowest R values occurred in UGA2K (0.3). ~~The highest value of R for surface~~
463 ~~temperature was found in ETH2K (0.6), followed by KEN2K (0.5) and UGA2K (0.3).~~ For wind speed, the highest
464 R coefficient value ~~is for KEN2K (0.5) and the lowest for UGA2K (0.1)~~ while for wind directions, the highest R
465 value found was for UGA2K (0.3) with values of approximately 0.2 for the other two domains (Table 3).

466
467 [Finally, the evaluation of the index of agreement \(IOA\) shows values for surface temperature between 0.31](#)
468 [\(KEN2K\) and 0.53 \(ETH2K\) and values between 0.44 and 0.47 for relative humidity in the three domains. For](#)
469 [wind speed and directions, the IOA varies between 0.39 \(UGA2K\) and 0.46 \(ETH2K\) for the former and between](#)
470 [0.26 \(UGA2K\) and 0.41 \(KEN2K\) for the latter.](#)

471 472 3.1.2 Hourly variation of Temperature and Relative humidity

473
474 The three MIDAS stations providing weather observations closest to the urban areas of the Addis Ababa, Kampala
475 and Nairobi have been analysed individually in form of hourly time series of surface temperature and relative
476 humidity and wind roses for wind speed and directions.

477
478 The hourly surface temperature and relative humidity are shown in Figure 4 for the three ground weather stations
479 closest to the centre of the three cities: Addis-Bole (n1 in Figure 3a), Kampala Station (n5 in Figure 3b) and
480 Nairobi (n7 in Figure 3c).

481
482 The temperature range observed at the three stations was between 9 and 27° C for the Addis-Bole Station, 16 and
483 31° C for Kampala and 16 and 33° C for Nairobi. By inspection of Figure 4, it can be seen that the WRF model
484 is able to reproduce the main diurnal cycle of variation of temperature and relative humidity for the three ground
485 weather stations. Surface temperature peaks are slightly underestimated by the model for the three stations with a
486 small mean bias at the three stations between -0.06 and -0.1° C. The highest agreement between the model and
487 observation is for Kampala while the model tends to underestimate the diurnal peaks of surface temperature almost
488 systematically for Addis-Bole and Nairobi stations.

489
490 [The mean relative humidity observed at the three stations shows different ranges of excursion from the model](#)
491 [predictions depending on the characteristics of the environment. The station of Addis-Bole shows the higher](#)
492 [variation from 15 to 98 %. Nairobi station from 17 to 98 % and Kampala from 19 to 99 %. From Figure 4, it may](#)
493 [be seen that relative humidity variations over time are correctly captured by WRF for the Nairobi and Addis-Bole](#)
494 [stations. Despite this both the diurnal peaks and night lowest values seems to be not correctly reproduced by the](#)
495 [model that tends to overestimate the formers and underestimate the latter with a bias between -0.1 and 0.004 %.](#)

496
497 [However, WRF appears systematically to underestimate the relative humidity for the Kampala station showing a](#)
498 [mean negative bias. Different reasons could affect the underestimation of the relative humidity at this station. The](#)

Deleted: H

Deleted: s

Deleted: were

Deleted: s

Deleted: are

Deleted: for

Deleted: the

Deleted: for

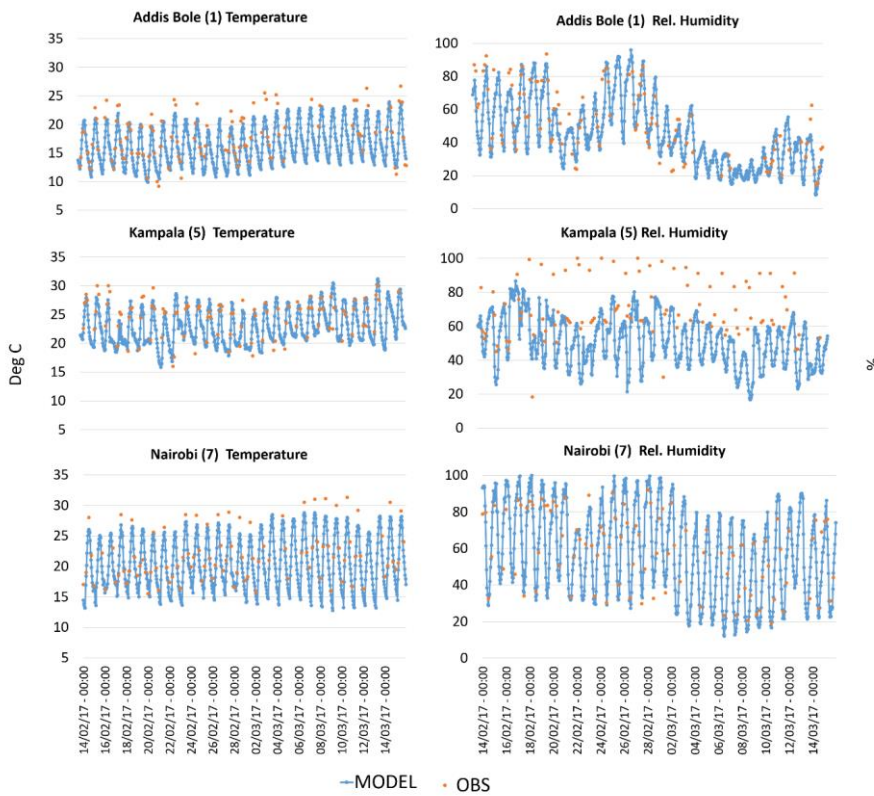
Deleted:

508 [sensitivity of WRF model to the land use data \(Teklay et al., 2019\) connected with the proximity of Kampala to](#)
 509 [Lake Victoria, which is a massive inland body of water \(surface area 68,800 km²\) could influence the local](#)
 510 [variation of relative humidity in ways which are not well reproduced by the model. The influence of Lake Victoria](#)
 511 [and of the Kampala's complex topography on measurements of relative humidity was previously highlighted by](#)
 512 [Singh et al. \(2020\) in relation to monthly visibility connected with PM levels. ~~It has to be noted that relative~~](#)
 513 [humidity was calculated from surface temperature and dew point values following Alduchov O. \(1996\) and not](#)
 514 [directly sampled. A better agreement in the simulation of relative humidity from WRF can be found in the station](#)
 515 [of Entebbe \(n4 in Figure 3b\) where the mean normalized bias shows a small underestimation of 0.04 %.](#)

Deleted: RH

Deleted: Noting

516



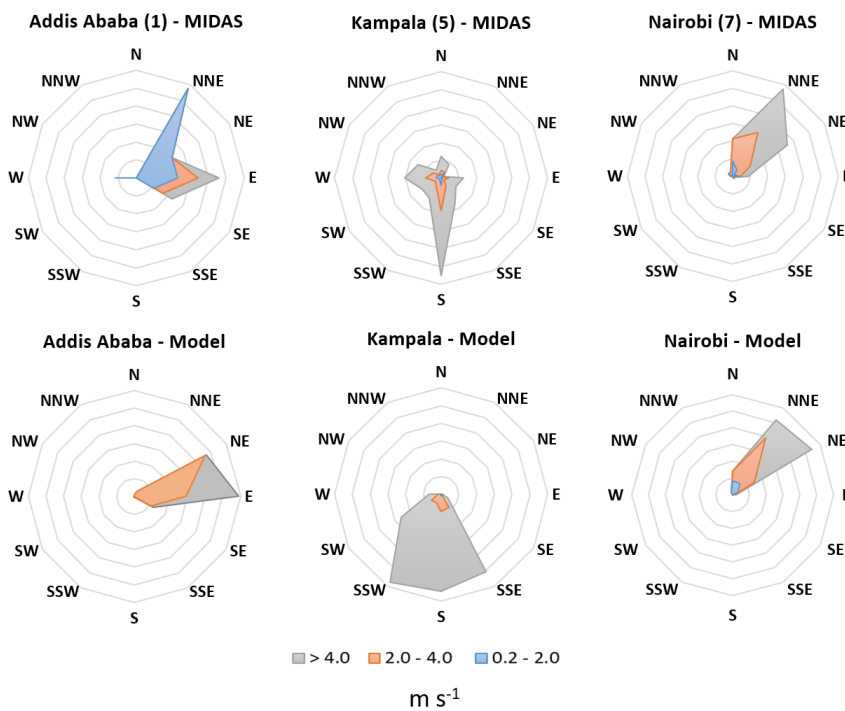
517 **Figure 4:** Hourly time series of surface temperature (left column) and relative humidity (right column) for the closest ground
 518 weather stations to the urban centres of the cities of Addis Ababa (station 1 in Figure 3a), Kampala (station 5 in Figure 3b)
 519 and Nairobi (station 7 in Figure 3c). Comparison between modelled values (blue lines) obtained from the 2x2km domains
 520 and hourly observations (orange spots) from MIDAS database.
 521
 522

523 [Wind speed and directions from the urban stations of Addis Bole \(n1 in Figure 3a\), Kampala Station \(n5 in Figure](#)
 524 [3b\) and Nairobi \(n7 in Figure 3c\) are shown in Figure 5 in the form of wind roses. WRF can reproduce the average](#)
 525 [wind directions in close agreement with the observed data for the analysed period for Nairobi showing the](#)

Deleted: -

529 predominance presence of North-North-Eastern winds with high speed ($> 4.0 \text{ m s}^{-1}$). Wind speed observations
 530 from the ground weather station of Kampala also suggest a strong southern wind component ($> 4.0 \text{ m s}^{-1}$) while
 531 the model seems to reproduce a similar magnitude of the wind speed but on a larger range of directions ranging
 532 from the South-South-East direction to South-South-West. For Addis Ababa, WRF seems able to capture and
 533 reproduce the main wind directions observed for the simulated period, e.g., Eastern and North-Eastern winds.
 534 Despite this, slower winds between 0.2 and 2.0 m s^{-1} with a strong North-Northeast component do not seem to be
 535 replicated by the model for the station located inside the capital of Ethiopia.

Deleted: Moreover, the model replicates the wind directions for Nairobi with higher agreement in comparison to Addis Ababa and Kampala.



536
 537 **Figure 5:** Averaged wind roses for the whole analysed period (14th of February to 14th of March 2017) from the closest ground
 538 weather stations to the urban centres of Nairobi (n7 in Figure 3c), Kampala (n5 in Figure 3b) and Addis Ababa (n1 in Figure
 539 3a) (MIDAS, top) and from WRF simulation outputs (Model, bottom).

540
 541 The lower agreement in the reproduction of the wind speed and direction in Addis Bole and Kampala stations can
 542 be connected to the particular locations of both stations. The difference in the location of the observations can, in
 543 fact, influence rapid changes in directions and speed locally recorded and not reproduced by the model. In the
 544 case of Kampala, the airport “Entebbe” is located near the coast of the Lake Victoria where the local conditions
 545 of wind are more susceptible of variation and can be erroneously reproduced by the model. In the case of Addis
 546 Bole, the only station settled in the urban area, the urban topography and possible canyon effects of the wind can

Deleted: that the station of Addis-Bole is the only one settled inside an urban area, while the stations of Kampala and Nairobi are settled in the respective airports located in peri-urban areas.

Deleted: have an

Deleted: on

Deleted: the

Deleted: in the observations

Deleted: These rapid changes given by the open spaces (airport), or...the the

Deleted: the

Deleted: of urban areas cannot

563 be not well captured by the model that reproduces a more constant range of wind speed and directions not
564 accounting for quick variations at low speed observed at the station.

Deleted: WRF that take in account of a differentiation of the land use between urban and not urban areas

565
566 The results obtained from the validation of the meteorological simulations performed over East African domains
567 using WRF show that the model is on average able to reproduce all four variables taken in account close to the
568 observed data in the 2×2 km domains with variable agreement between the three cities. The highest agreement in
569 the weather analysis has been found for surface temperature with similar biases to Kerandi et al. (2017) and
570 relative humidity similar to Pohl et al. (2011), which is sufficiently accurate to be able to use these values for the
571 physical calculations done by the chemistry transport model.

572
573 Nevertheless, the more detailed analysis of the urban weather stations revealed discrepancies in the reproduction
574 of relative humidity and wind direction for the station of Kampala (UGA2K) that could affect the deposition,
575 removal and transport processes simulated by CHIMERE and will be object of future investigation to further
576 improve the meteorological performance of WRF. However, for the purposes of the present work the range of
577 bias found for the meteorological variables can be considered acceptable. Even if the bias found for some variable
578 in the calculation of the averaged statistics over all stations was high, the individual weather stations close to the
579 urban areas of interest showed smaller bias and levels of MFB and MFE inside the goal or criteria range of
580 performance and therefore considered acceptable for simulations.

581 **3.2 Validation of CHIMERE simulations**

582
583
584 The CHIMERE validation has been focused on the hourly levels of PM_{2.5} modelled at the two observation sites
585 for the domain KEN2K, representative of a roadside site and a rural background site. Also, from the urban
586 background observational sites of the U.S. Embassies of Kampala (UGA2K) and Addis Ababa (ETH2K). The
587 performance of CHIMERE was analysed also in terms of mean fractional error (MFE), mean fractional bias
588 (MFB) and Pearson's coefficient (R) against the different level of average concentrations of PM_{2.5} in the four
589 observation points to evaluate the response of the model in reproducing low and high levels of hourly
590 concentrations in comparison with observed values.

591
592 The validation of CHIMERE was done for the domains at highest resolution (2×2 km) despite the availability of
593 emissions at a similar spatial resolution. The reason of this choice is motivated by the necessity to validate the
594 reliability of the model against observation data from particular locations in different backgrounds. In order to
595 better configure the model to represent the different urban and rural environments it is necessary to take in account
596 the uncertainties of a model representation against an observation point. One cause of uncertainty when comparing
597 modelling outputs with observations is the difference between a point measurement and a volumetric grid cell
598 averaged modelled concentration (Seinfeld, 2016). On one hand, the extent of a measurement point, in fact,
599 represents only the extent of the nearby points or an average concentration in a specified area. On the other hand,
600 a surface level modelling grid typically has highest resolution of 1 km with a vertical height of between 20 and
601 40 m and the concentration represented by the model is the average over the entire grid cell.

605 [In the particular case of the domains of East Africa, CHIMERE simulates at coarse resolution e.g., the 6×6 km,](#)
606 [values of concentration representative of an average of 36 km², difficult to be compared with observations taken](#)
607 [in a particular point. Increasing the spatial resolution and bringing it to 2×2 km the average value inside each grid](#)
608 [cell will be representative of a smaller area such as 4 km² whose average value can be closer compared with an](#)
609 [individual observation point.](#)

611 3.2.1 Statistical evaluation of model performances

612 The absolute bias between mean observed and modelled concentrations of PM_{2.5} shows an overestimation of the
613 model for the domain KEN2K by between 0.01 and 3.7 µg m⁻³ for Nanyuki and Nairobi, respectively, and for
614 Addis Ababa (0.6 µg m⁻³). On the contrary, the model underestimates PM_{2.5} for the domain UGA2K (Kampala)
615 by 7.2 µg m⁻³ (Table 4).
616

Deleted: 6

617 [The mean fractional bias \(MFB\) and error \(MFE\) for the two Kenyan observation points were found in both cases](#)
618 [inside the goal performance criteria with MFE < 50% and MFB ≤ ± 30% both in Nairobi \(roadside site\) and in](#)
619 [Nanyuki \(rural site\). The hourly MFB and MFE were 4.88 and 25.39 for Nairobi and 3.36 and 8.33 for Nanyuki](#)
620 [while 0.1 and 1.99 for Nairobi and 1.08 and 4.73 for Nanyuki were the respective values found for the daily](#)
621 [analysis.](#)

622 [The MFB and MFE analysis for the urban background site in Addis Ababa showed values inside the range of the](#)
623 [goal criteria both for the hourly \(2.93 and 29.99 for MFB and MFE\) and for daily analysis \(8.23 and 2.86\). Finally,](#)
624 [in the urban background site of Kampala the MFB were found inside the goal criteria both for daily \(-11.28\) and](#)
625 [hourly \(-7.60\) analysis, while for the MFE the hourly analysis showed a value in the range of the criteria range](#)
626 [\(32.99\) but daily MFE in the goal performance range \(22.06\) \(Table 4\).](#)
627

628 The highest Pearson's coefficients (R) were found in Nanyuki with hourly and daily values of between 0.91 and
629 0.93. The roadside site of Tom Mboya Street in Nairobi had R values of between 0.35 and 0.38 while the urban
630 background sites of Addis Ababa and Kampala had a lower agreement an hourly level (R values were between
631 0.10 and 0.29, respectively) than at a daily level (R values of between 0.42 and 0.30, respectively).
632

633 [In general, the statistical analysis demonstrates that the model can reproduce the daily pattern of the hourly](#)
634 [changes in concentrations for the two pollutants both in the three urban/roadside sites and in the rural site](#)
635 [considered. The low R coefficient values obtained for the urban domains at the hourly level suggests that sources](#)
636 [of anthropogenic emissions affecting urban air quality are still missing from the current emission inventory.](#)
637 [Further work will be focused on the improvement of the magnitude of the emissions to better match the observed](#)
638 [levels of concentrations of particulate matter at the urban level. Despite this and considering the daily average](#)
639 [concentrations in the urban sites, the R coefficients were found to be between 30 and 42 % suggesting that](#)
640 [CHIMERE better reproduces the concentrations of PM_{2.5} using daily averaging.](#)
641
642
643

The performance of CHIMERE varies between the domains of Kenya, Uganda, and Ethiopia. The performance of the model has been optimised during the validation for the simulation of hourly concentrations of PM_{2.5} in Kenya and the same configuration applied to the domain of Uganda and Ethiopia to compare the reliability of the model. The difference in performance can be connected to different reasons: In first place, the difference in the sampling methods used for the two sites in Kenya against the measurements taken in the U.S. Embassies of Kampala and Addis Ababa. Secondly, another element of differentiation can be connected to the location of the observation sites in the cases of the U.S. Embassies and/or the possible influence of local sources not accounted in the emission inventories.

Deleted: ¶

Table 4: Hourly and daily statistical evaluation of CHIMERE model performance for the cities of Nairobi against ASAP observed data and against U.S. Embassies data for the cities of Addis Ababa and Kampala.

| ASAP OBS | NAIROBI PM _{2.5} (µg/m ³) roadside | | NANYUKI PM _{2.5} (µg/m ³) rural | |
|------------------|---------------------------------------------------------|--------|--------------------------------------------------------|--------|
| | DAILY | HOURLY | DAILY | HOURLY |
| Mean MOD | 58.3 | 58.3 | 3.24 | 3.24 |
| Mean OBS | 54.6 | 54.6 | 3.23 | 3.23 |
| MFB | 0.1 | 4.88 | 1.08 | 3.36 |
| MFE | 1.99 | 25.39 | 4.73 | 8.33 |
| R | 0.38 | 0.35 | 0.93 | 0.91 |
| U.S. EMBASSY OBS | ADDIS A. – PM _{2.5} (µg/m ³) urban | | KAMPALA – PM _{2.5} (µg/m ³) urban | |
| | DAILY | HOURLY | DAILY | HOURLY |
| Mean MOD | 18.7 | 18.7 | 36.2 | 36.2 |
| Mean OBS | 18.1 | 18.1 | 43.4 | 43.4 |
| MFB | 8.23 | 2.93 | -11.28 | -7.60 |
| MFE | 2.86 | 29.99 | 22.06 | 32.99 |
| R | 0.42 | 0.10 | 0.30 | 0.29 |

Finally, the site of Nanyuki is the location where the agreement between model and observations is highest. This site was chosen by Pope et al. (2018) as rural spot in a location of minimum local air pollution useful to calculate the net urban increment subtracting the rural background concentrations of Nanyuki from the urban concentrations in Nairobi. Is therefore intended by their work that the average concentrations in that site were really low. The model is able to reproduce this low level of contamination close to the reality and to reproduce also peaks of contamination in particular days of February probably generated elsewhere (see Section 3.2.2).

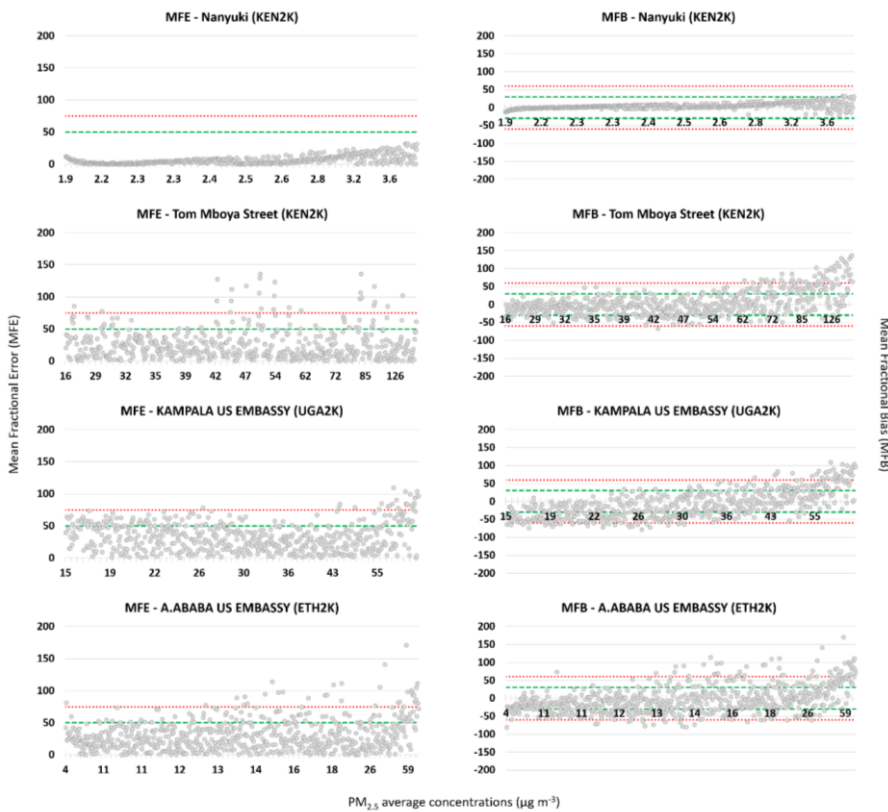
The MFB and MFE analysis have been conducted also at hourly level comparing modelling outputs and observations from all six sites in relation to the magnitude of hourly concentrations (Figure 6).

Deleted: has

There are some MFB values outside the criteria range for PM_{2.5} for the urban sites of Addis Ababa and Kampala and for the roadside site of Tom Mboya Street in Nairobi. In terms of the upper limit (MFB > 60 %) these values tend to be concentrated between 60 and 130 µg m⁻³ for Tom Mboya Street, 40 and 55 µg m⁻³ for Kampala and between 13 and 59 µg m⁻³ for Addis Ababa (Figure 6). A much smaller number of MFB values for the Addis Ababa and Kampala sites are less than the lower criteria limit and these tend to be for lower concentrations between 10 and 26 µg m⁻³.

676
 677
 678
 679
 680
 681
 682

MFE values outside the ranges of criteria are between 42-55 and 80-130 $\mu\text{g m}^{-3}$ for Tom Mboya Street, 43 and 60 $\mu\text{g m}^{-3}$ for Kampala and 13 and 59 $\mu\text{g m}^{-3}$ for Addis Ababa (Figure 6). The latter two sites present a more variability of MFB and MFE in comparison with the two sites of Kenya where is visible a common positive bias of the model in reproducing the highest concentration levels. The reliability of the model is therefore higher for the domain of Kenya, both for a rural and for a roadside site than for the two urban background sites in Uganda and Ethiopia.



683
 684
 685
 686
 687
 688
 689

Figure 6: Hourly mean fractional bias (MFB) and mean fractional error (MFE) values calculated for the locations of Tom Mboya Street and Nanyuki (KEN2K), Kampala U.S. Embassy (UGA2K) and Addis Ababa U.S. Embassy (ETH2K) for the analysed period against hourly concentrations of PM_{2.5}. The green lines represent the MFB range $\pm 30\%$ and the MFE limit of 50% for which the model performance can be considered reliable, the red lines represent the MFB range $\pm 60\%$ and the MFE limit of 75% for which model performance can be increased by diagnostic analysis on the chemical precursors of PM_{2.5}.

690 The overall performance of the model against different levels of concentrations is summarised in Table 5. The
 691 PM_{2.5} reproduced at the two sites in KEN2K shows a higher percentage of values within the MFB and MFE
 692 performance goals for the rural site of Nanyuki, than for Tom Mboya Street. *e.g.*, 97 % compared to 69 % and 99
 693 % compared to 88 % for the MFB and MFE measures respectively. For the criteria measure, the corresponding
 694 percentages are 2 % vs. 22 % and 1 vs. 7 % (Table 5).

695
 696 The percentages for the urban sites of Kampala and Addis Ababa show a lower agreement between the model and
 697 observations. For the former 48 % of the values according to the MFB measure are within the goal range, 37 %
 698 are within the criteria range and 15 % are outside. For the latter, according to the MFB criteria, 57 % of the values
 699 are inside the goal range, 30 % of values are within the criteria range and 13 % are outside. In terms of the MFE
 700 measure, 74 % and 80 % of values for the two cities are within the goal range, 16 % and 11 % within the criteria
 701 range and 10 % and 9 % outside respectively (Table 5).

702
 703 **Table 5:** Hourly mean fractional bias (MFB) and error (MFE) percentage of points inside the goal limit (GOAL), inside the
 704 diagnostic range (CRITERIA) and outside the reliability criteria (OUT) from model outputs extracted from the four analysed
 705 locations.

| City | MFB | | | MFE | | |
|-----------------------|----------|--------------|---------|----------|--------------|---------|
| | GOAL (%) | CRITERIA (%) | OUT (%) | GOAL (%) | CRITERIA (%) | OUT (%) |
| Tom Mboya St. (KEN2K) | 69 | 22 | 9 | 88 | 7 | 5 |
| Nanyuki (KEN2K) | 97 | 2 | 1 | 99 | 1 | 0 |
| Kampala (UGA2K) | 48 | 37 | 15 | 74 | 16 | 10 |
| A. Ababa (ETH2K) | 57 | 30 | 13 | 80 | 11 | 9 |

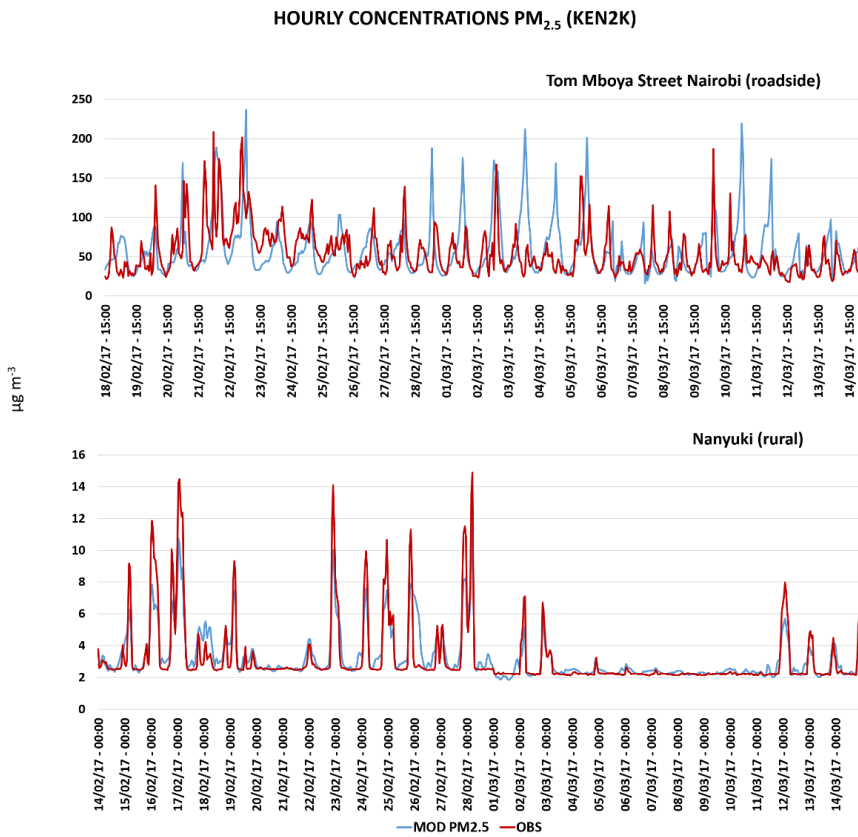
706
 707 According to the methodology proposed by (Boylan and Russel, 2006) the performance of a modelling system is
 708 fairly good for PM_{2.5} representation if about the 50 % of the points are within the goal range and a large majority
 709 are within the criteria range. From the analysis of the four sampling sites the values of MFB inside both the goal
 710 and range for Tom Mboya Street are 69 %, 97 % for Nanyuki and 57 % for Addis Ababa and only for Kampala
 711 are 48 %. Similarly, for the MFE measure, 99 % for Nanyuki, 88 % for Tom Mboya Street, 80 % for Addis Ababa
 712 and 74 % for Kampala are inside both the goal range. The demonstrates that the performance of the model can be
 713 considered to be satisfactory (Table 5).

714
 715 Finally, the reason for the presence in the Addis Ababa and Kampala simulations of values outside the criteria
 716 range both at high and at low concentrations of PM_{2.5} can be connected to the representation of the original PM
 717 emissions in the combined inventory. It is possible that CHIMERE is not able to correctly reproduce all the
 718 chemical processes involved in the secondary formation of inorganic and organic individual components of PM_{2.5}
 719 with the extent of the present input data. Moreover, the possible misrepresentation of local emission sources not
 720 reproduced in DICE-EDGAR can also affect the performance of the model. Finally, the different location of the
 721 urban background observation sites and the sampling techniques for PM observation can also have a key role in
 722 the correct detection of the concentrations.

723
 724 **3.2.3 Hourly variation of PM_{2.5} in urban and rural sites of Kenya**
 725

726 Hourly modelled variation of PM_{2.5} levels obtained by CHIMERE compared with observations are shown for the
 727 urban sampling site of Tom Mboya Street in Nairobi and for the rural site of Nanyuki (Figure 3c).

728



729
 730 **Figure 7:** Hourly time series for PM_{2.5} from the roadside of Tom Mboya Street (top) and from the rural site of Nanyuki (bottom)
 731 from modelled output from CHIMERE model (blue line) and observed values from Pope et al. (2018) (red line) for the analysed
 732 period. The simulation started on the 14th of February. For the Tom Mboya Street site only the period of time between the 18th
 733 of February and the 14th of March when observations were available has been shown in the timeseries.
 734

735 By inspection of Figure 7 it can be seen that CHIMERE is able, in general, to reproduce the daily variation of
 736 PM_{2.5} across the simulated period at both sites. The magnitude of the emissions adopted seems to be suitable both
 737 for the roadside area of Tom Mboya Street and for the rural background site of Nanyuki, with higher agreement
 738 shown by the latter. CHIMERE captures only part of the daily peak observed in Tom Mboya Street with
 739 comparable magnitude but misrepresents some peaks. In particular it models higher hourly peaks than those
 740 observed as previously mentioned in the MFB and MFE analysis.
 741

742 The misrepresentation of some high peaks in Tom Mboya Street is possibly due to a number of different reasons.
 743 Firstly, it is important to recall that the point measurements and relative observed concentrations are representative
 744 of a smaller portion of space in comparison with grid-cell concentrations modelled. In this particular case the
 745 comparison is between a roadside site subjected to possible additional local sources of PM_{2.5} not accounted for in

746 the emissions and not correctly reproduced by CHIMERE. On the other hand, a few of the modelled peaks were
747 overestimated. This can be addressed by improved temporal description of the emissions and in their magnitude
748 in comparison to the reality. As mentioned previously, the anthropogenic emissions used in this work were the
749 most up-to-date available at the time and that there is inevitably some difference between the measured data due
750 to the difference in time between the inventories and the measurements. Despite this, there is reasonable agreement
751 between model outputs and observed concentrations for the majority of the analysed period highlighting the
752 reliability of CHIMERE in describing the hourly concentrations trends for a roadside site with expected high
753 levels of PM_{2.5} contamination.

754
755 Similarly, in the rural site of Nanyuki, the model seems to correctly reproduce the hourly variation of the
756 concentrations during the whole period, underestimating the maximum peaks at the beginning of February and in
757 the last four days of simulation in March. (Figure 7). The site shows different magnitude in the concentrations of
758 PM_{2.5} when comparing the February and March periods. While between the 4th and the 10th of March hourly
759 concentrations are around 3-4 µg m⁻³, previously and subsequently to this period of time, the concentrations of
760 PM_{2.5} are more than two times higher. This behaviour is visible both in the observations from the site (red line in
761 Figure 7, bottom) and from the model outputs obtained using CHIMERE (blue line in Figure 7, bottom).

762
763 One of the few possible reasons for this different behaviour may be connected to dispersion of pollutants in
764 particular weather conditions of wind speed and wind directions during February and March in the area. To
765 investigate this possible explanation we consider the closest MIDAS weather station to the sampling area of
766 Nanyuki, in the town of Nyeri (0.43°S, 36.95°E altitude 1916 m a.g.l.) (n10 in Figure 3). Nyeri is only 60 km
767 from the Nanyuki site and is situated between Mount Kenya (0.10°S, 37.30°E, altitude 4341 m a.g.l.) to the west
768 and the Aberdare Range (0.46°S, 36.69°E, altitude 3441 m a.g.l.).

769
770 The daily average concentrations observed in the sampling site of Nanyuki have been compared with the daily
771 mean values of wind speed and directions observed at the MIDAS station of Nyeri and with the daily mean values
772 of wind speed and directions modelled by WRF in Nanyuki (Figure 8). The period between the 4th and the 10th of
773 March, when the daily average concentrations of PM_{2.5} observed in Nanyuki were around 2.2 µg m⁻³ corresponds
774 to higher wind speed conditions (between 4 and 5 m s⁻¹) mainly coming from North-Est (around 60 degrees). In
775 the same period, at Nyeri the modelled wind speed was low (between 1 and 2.5 m s⁻¹) and mainly with a westerly
776 component (between 220 and 300 degrees).

777
778 In the periods of higher average daily concentrations of PM_{2.5} between the 15th and the 19th and between 22nd and
779 the 28th of February 2017, both in Nyeri (using observations) and in Nanyuki (using model outputs) the component
780 of wind directions seems to be consistent in reproducing southern winds (between 120 and 190 degrees) with wind
781 speeds between 1.5 and 2.5 m s⁻¹ in the first period and between 2 and 3 m s⁻¹ in the second period.

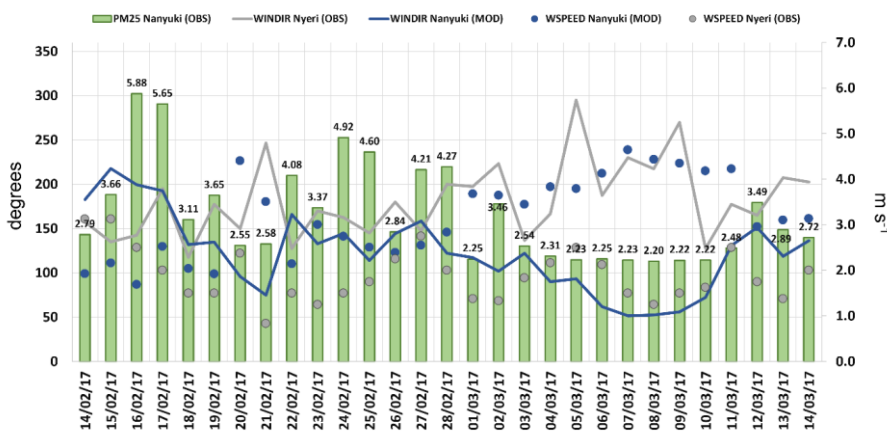
782
783 The correspondence between the wind speed and directions in particular time periods and the vicinity of the towns
784 could suggest the potential dispersion of pollutants from the southern area where the hotspot of Nyeri is located
785 upwind in the northern area of Nanyuki (downwind) in accordance with the wind fluxes from south to north from

Deleted: T

Deleted: is

788 Nyeri from the observations and also from WRF outputs extracted from the Nanyuki location. The flux could also
 789 be driven by the location of Nyeri sited at the entrance of a basin between two mountain ranges. On the other
 790 hand, in the period of low concentrations between the 4th and the 10th of March, northeaster winds (around 60
 791 degrees) blow with high speed on Nanyuki (around 4 m s⁻²) while lower speed winds (between 1 and 2 m s⁻²) from
 792 a more variable directions (between 170 and 300 degrees) are blow in Nyeri preventing the possible dispersion of
 793 pollutants.

Deleted: northeaster



794
 795 **Figure 8:** Comparison between daily observed values of wind speed (grey spots) directions (grey lines) from the MIDAS site
 796 of Nyeri (n10 in Figure 3), modelled daily wind speed (blue dots) and directions (blue lines) from the site of Nanyuki with
 797 daily average observations of PM_{2.5} (expressed in µg m⁻³, green columns) obtained from the sampling site of Nanyuki (red dot
 798 in Figure 3c).

Deleted: .

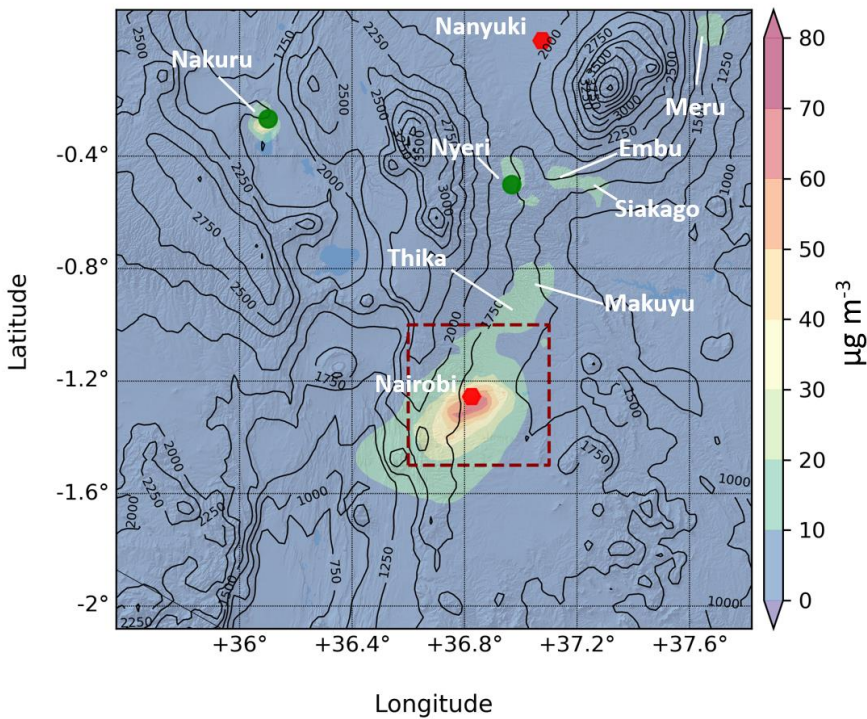
800 The present analysis was done on the relationships between weather conditions and the relative correspondence
 801 in hourly and daily levels of PM_{2.5}. Further analyses are necessary to clarify the possible presence of additional or
 802 alternative factors influencing the changes in concentrations observed and modelled by CHIMERE. The presence
 803 of possible precipitations during the low concentration period could represent an alternative possibility the change
 804 in concentrations. Despite this no precipitation were recorded during that period according to Pope et al. (2018)
 805 and no precipitation was modelled by WRF in that time period. Nevertheless, the lack of additional weather
 806 observations in the sampling site of Nanyuki and middle way between the two towns prevent from any additional
 807 hypothesis in relation to the presence of possible pollutant transport phenomena that will be object of future
 808 investigations. Further efforts will be oriented in a more detailed trajectory analysis of the winds and in a more
 809 detailed representation of the emissive sources present in the area to investigate possible transport effects in this
 810 area.

Deleted: investigate

811
 812 The average concentrations of PM_{2.5} for the entire period of simulation between the 14th of February and 14th of
 813 March 2017 are shown for the domain centred over Kenya with spatial resolution of 2×2 km (KEN2K, Figure 9).
 814 Highest average concentrations during the monthly period are modelled in the urban area of Nairobi (defined by

818 the red dashed square in Figure 9) with highest average values inside the city around $80 \mu\text{g m}^{-3}$. The concentrations
 819 are spread on average in the southwest area of the city and on the northeast side in direction of the conurbation of
 820 Thika and Makuyu. These towns became part of the Metropolitan Area of Nairobi in 2008 due to the rapid increase
 821 in population and urbanization of the area (UNEP, 2009) and represent a large hotspot of emissions of $\text{PM}_{2.5}$
 822 with concentrations modelled between 20 and $30 \mu\text{g m}^{-3}$ as average of the entire period. Other hotspots of
 823 concentration of $\text{PM}_{2.5}$ found in the domain are the city of Nakuru with average concentrations between 20 and
 824 $40 \mu\text{g m}^{-3}$ and the area between Nyeri, Embu, Meru and Siakago with average concentrations around 20 and 30
 825 $\mu\text{g m}^{-3}$ (Figure 9). The average of the modelled concentrations in the area of Nanyuki is generally smaller, with
 826 concentration not exceeding $10 \mu\text{g m}^{-3}$ in the whole area.

Deleted: j



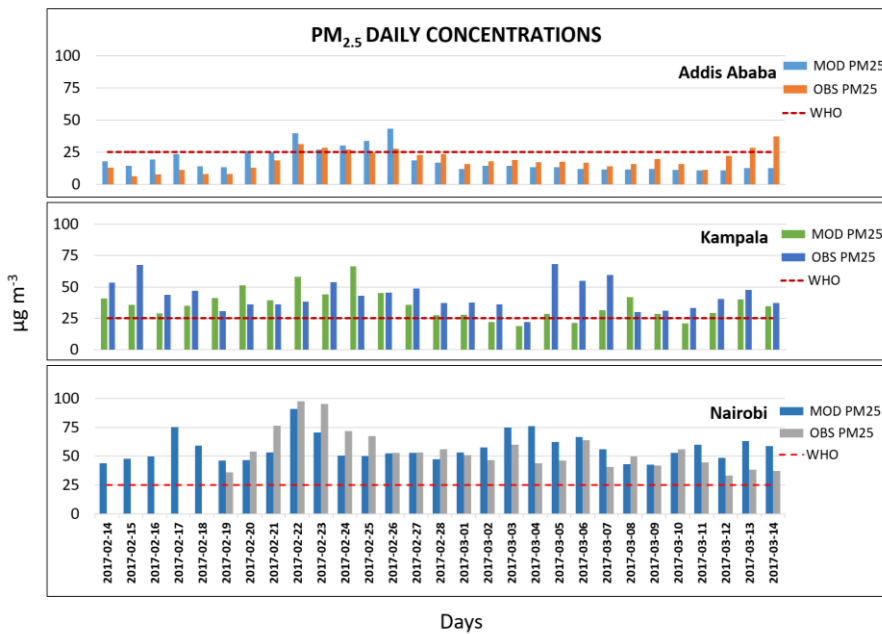
828
 829 **Figure 9:** Average concentration of $\text{PM}_{2.5}$ for the whole simulated period for the domain KEN2K at spatial resolution of 2×2
 830 km. The map shows the location of the hotspots with higher average concentrations modelled by CHIMERE for the entire
 831 period. The red dashed square shows the urban domain of Nairobi analysed for the Air Quality Indexes analysis in section
 832 3.3.

833 **3.3 CHIMERE as an Air Quality Management Tool**

Deleted: ¶

834
 835 The usefulness of CHIMERE as a decision support tool to facilitate air quality management of large urban
 836 conurbations of SSEA was investigated for the three domains at a resolution of 2×2 km, namely: KEN2K, UGA2K

839 and ETH2K. Daily observations of PM_{2.5} for the three domains were compared with modelled concentrations in
 840 terms of number of exceedances from the WHO limit of 25 µg m⁻³ observed and captured by the model (Figure
 841 10). For the limited case of Nairobi, hourly average concentrations for the whole monitored period were compared
 842 with Air Quality Indexes data and the spatial distribution of daily average concentrations on the constituencies
 843 was analysed, highlighting how many areas of the city showed low air quality indexes during the analysed period
 844 (Figure 11).



845 **Figure 10:** Daily concentrations of PM_{2.5} between the 14th of February and 14th of March obtained from CHIMERE outputs
 846 from domains at 2x2 km compared with US Embassy daily totals for the cities of Addis Ababa (top) and Kampala (middles)
 847 and with ASAP observations for the city of Nairobi (bottom). All three simulations have been compared also with the WHO
 848 threshold limit for PM_{2.5} concentrations (red line). For the case of Nairobi, only observations from the 18th of February were
 849 available.
 850
 851

852 Daily concentrations of PM_{2.5} modelled by CHIMERE were compared with the number of exceedances of the
 853 WHO limit (e.g., 25 µg m⁻³) observed during the simulated period. Figure 10 shows the daily average
 854 concentrations for the three cities in the sampling sites used for the validation of the model. It can be seen that
 855 Nairobi and Kampala have the highest number of exceedances from the WHO limits (24) followed by Addis
 856 Ababa with only 6 observed exceedances. From Table 6 it can be seen that CHIMERE provides sufficient accuracy
 857 to detect the exceedances of PM_{2.5} from the WHO limits. In particular, it was able to detect 67 % of the exceedance
 858 for Addis Ababa with only two false positives, 91 % for Kampala and all of the exceedances for Nairobi without
 859 any false positives.

860 The Air Quality Index (AQI) represents the conversion of concentrations for fine particles such as PM_{2.5} to a
 861 number on a scale from 0 to 500 (Table 7). The higher the AQI value, the greater the level of air pollution and the
 862

863 greater the health concern. AQI values at or below 100 are generally thought of as satisfactory. When AQI values
 864 are above 100, air quality is unhealthy: at first for certain sensitive groups of people (101 – 150), then for everyone
 865 as AQI values get higher (>151) (EPA, 2012).
 866

867 **Table 6:** Summary of the number of WHO exceeding limits for PM_{2.5} during the simulated period from the 14th of February to
 868 the 14th of March 2017 observed and modelled. Ratio between the observed and modelled Exceeding limit and number of
 869 model overestimations are also reported.

| Domains | WHO Exceeding Limits (obs) | WHO Exceeding Limits (mod) | Ratio (%) | Model False positive |
|-------------|----------------------------|----------------------------|-----------|----------------------|
| Nairobi | 24 | 24 | 100 | 0 |
| Addis Ababa | 6 | 4 | 67 | 2 |
| Kampala | 24 | 22 | 91 | 0 |

870
 871 The daily average concentrations of PM_{2.5} during the analysed period between the 14th of February and 14th of
 872 March 2017 have been averaged for the urban area of Nairobi (red square in Figure 9 and Figure 11) and compared
 873 with the city constituencies spatial extension according to data from the Open Africa dataset (Open-Africa, 2018).
 874 According to the division, 17 are the constituencies inside the Nairobi city boundaries (Figure 11). Averaged daily
 875 concentrations of PM_{2.5} show that 8 of 17 constituencies had AQI values between 55.5 - 150.4 µg m⁻³ during the
 876 whole period. These areas are the most central and urbanized of Nairobi. Starehe constituency (n13 in Figure 11)
 877 contains the Tom Mboya Street sampling site (black spot in Figure 11) previously discussed where the WHO
 878 limits for PM_{2.5} have been systematically exceeded during the analysed period. According to the SEDAC
 879 population density data this area has population density between 15,000 and 30,000 people/km² exposed to AQI
 880 between 151-200 corresponding to unhealthy category for human health. Finally, the Langata constituency
 881 (magenta spot in Figure 11) has a population of 176,000 people and shows average levels of PM_{2.5} of 45 µg m⁻³,
 882 unhealthy for sensitive groups of people.
 883

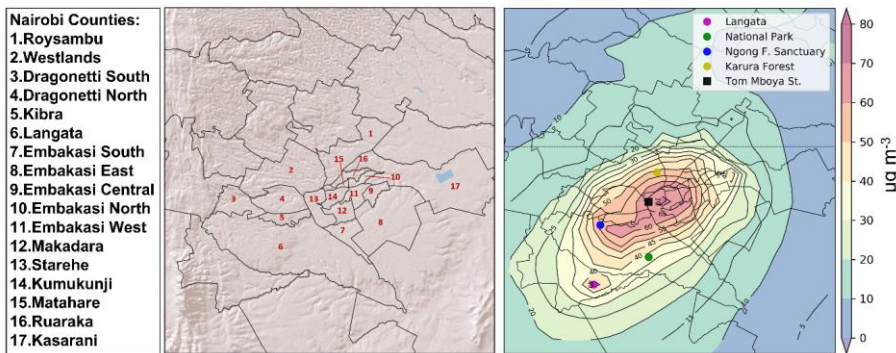
884 **Table 7:** Air Quality Index categories and relative range of 24-hour average concentrations for PM_{2.5} reported by the US
 885 EPA revised air quality standard for particle pollution of 2012 (EPA, 2012)

| AQI Category | Index values | AQI Breakpoints (µg m ⁻³ on 24-hour average) |
|--------------------------------|--------------|---------------------------------------------------------|
| Good | 0 - 50 | 0.0 - 12.0 |
| Moderate | 51 - 100 | 12.1 - 35.4 |
| Unhealthy for sensitive Groups | 101 - 150 | 35.5 - 55.4 |
| Unhealthy | 151 - 200 | 55.5 - 150.4 |
| Very Unhealthy | 201 - 300 | 150.5 - 250.4 |
| Hazardous | >301 | >250.5 |

886
 887 Moreover, Nairobi has a number of natural areas on the outskirts of city. Some particular locations such as the
 888 Karura Forest (yellow spot in Figure 11) and the Ngong Forest Sanctuary (blue spot in Figure 11) show averaged
 889 daily levels of PM_{2.5} around 50 and 55 µg m⁻³ corresponding to an AQI of between 101 and 150 (e.g., unhealthy
 890 for certain sensitive groups of people). According to SEDAC data, the population density is between 10,000 and
 891 15,000 people/km² in this area. Similarly, in the south side, near the entrance to the Nairobi National Park (1.36°
 892 S, 36.82° E, green spot in Figure 11) the average daily levels of PM_{2.5} are approximately 40 µg m⁻³ with AQI
 893 values between 101 and 150 with a population density around 10,000 people/km². This area (surface area 117

894 km²) has been impacted by a rapid urbanization since 1973 with a consequent increase of human activities
 895 including settlement, pastoralism and agriculture (Ogega O.M., 2019). These activities have already made it
 896 difficult for wildlife to migrate to and from the Nairobi National Park also are resulting in a deterioration of air
 897 quality. The rapid increase of population density in the south side of Nairobi seriously risk increasing the level or
 898 AQI exposing more people to harmful level of PM_{2.5}.

899



900
 901 **Figure 11:** Map showing the urban area of the city of Nairobi shown as dashed square in Figure 9. The constituency division
 902 of Nairobi (left) from Open Africa dataset (Open Africa, 2018) is compared with the average hourly concentrations of PM_{2.5}
 903 over the analysed period (right).

Deleted: image

904 **4 Conclusions**

905
 906
 907 [The WRF and CHIMERE models were configured and validated to simulate the air quality levels of PM in Eastern](#)
 908 [Sub-Saharan African urban conurbations.](#)

909
 910 In order to obtain updated anthropogenic emissions for 2017, the global EDGAR inventory and the DICE
 911 inventory for Africa were merged and spatially distributed using population density data for the year 2017
 912 obtained by linear extrapolation.

913
 914 WRF showed a variable capability in reproducing the main surface weather patterns according to the different
 915 conditions of the three domains. A lower agreement between observations and the model was observed in Kampala
 916 for relative humidity and wind speed. The analysis was carried out on all surface meteorological stations available
 917 from the MIDAS network on a three-hourly basis. A further meteorological analysis extended to vertical profiles
 918 could reveal possible limitations of the model. However, the absence of vertical meteorological data limited the
 919 analysis and validation to ground level only.

920
 921 CHIMERE was able to reproduce the daily levels of PM_{2.5} for the urban site of Nairobi as well as for the rural site
 922 of Nanyuki. The 69 % of the MFB values and 88 % of the MFE value were inside the highest confidence area for
 923 Nairobi and the 97 % and 99 % for Nanyuki attesting that the agreement between the observed and modelled data

925 was sufficient to allow for quantitative analyses of daily average concentrations. Similar findings were also found
926 for the other two urban background domains of Addis Ababa (57 % for MFB and 80 % for MFE) and Kampala
927 (48% for MFB and 74 % for MFE) despite different characteristics and sources of observation being used for the
928 validation. The discrepancies observed in the hourly trends of PM_{2.5} modelled by CHIMERE compared to
929 observed values in the urban sites suggest that further studies are needed in the three urban areas. These studies
930 are required to improve the understanding of the typology and quantity of local emission sources, which are
931 sometimes misrepresented or absent in global emission inventories. This will enable the chemical processes acting
932 in the urban troposphere to be adequately characterised and thereby actual air quality levels to be determined.

933
934 Nevertheless, using existing data sets, CHIMERE has shown reliability in reproducing both hourly and daily levels
935 of PM_{2.5} with hourly values largely inside the range of reliability connected with mean fractional bias and error.

936 The merged emission inventory DICE-EDGAR, despite the low resolution was able to return a correct magnitude
937 for the emissions in representation of urban and rural context. Despite this, few urban peaks observed in Nairobi
938 have been missed by CHIMERE or in other cases misrepresented highlighting the necessity of further efforts in
939 the creation of newer emission inventories for SSEA. In the light of this, the possibility to develop local emission
940 inventories, ideally at high spatial resolution it would represent a significant step ahead in the air quality research
941 in this area of the world. Despite this and at the extent of the present data, CHIMERE showed enough robustness
942 and reliability to be adopted as a decision support tool for the management of air quality, correctly reproducing
943 most of the exceedances of the limits set by the WHO for PM_{2.5} for all three cities considered.

944
945 The analysis focused on the average concentrations of PM_{2.5} for the domain of Kenya revealed that the
946 metropolitan area of Nairobi represents a big hotspot of air pollution but that also small cities located in the
947 outskirts of the capital of Kenya showed worrying levels of atmospheric contamination. These levels of air
948 pollution have the potential capability to affect also rural areas where the local emissions are rare or not present.
949 The possibility of transport phenomena of PM_{2.5} towards these areas, however, is still to be verified. The work
950 has also shown for urban area of Nairobi the presence of low and unhealthy air quality indexes in 8 of 17 its
951 constituencies and the relative population density exposed to harmful level of air contamination. Moreover, a
952 number of natural areas in the outskirts of Nairobi have similarly low levels of AQI and increasing population
953 highlighting how the problem of poor urban air quality due to rapid urbanisation, anthropogenic activities and
954 lack of regulation can also detrimentally affect and deteriorate natural habitats.

955
956 Future efforts to improve the calibration and validation of the modelling system, especially relating to
957 meteorology, will focus on assessing the dispersion dynamics of contaminants through urban centres and possible
958 pollution transport events from urban to rural areas. To aid this, further work is required by local East African
959 authorities and research bodies to improve the quantity and the quality of data for weather and air quality
960 simulations. However, in this work, we have shown that currently available data is sufficient to carry out
961 simulations of air quality that can be used for quantitative evaluation of anthropogenic emissions impact and to
962 support mitigation policies at the local level.

963

964 **Authors Contribution:** **Andrea Mazzeo:** Conceptualization, Methodology, Software, Validation, Writing-
965 Original draft preparation, Writing- Reviewing and Editing. **Michael Burrow:** Supervision, Writing - Review &
966 Editing **Andrew Quinn:** Supervision, Resources. **Eloise A. Marais:** Data curation, Resources, Writing - Review
967 and Editing. **Ajit Singh:** Resources, **David N'gang'a:** Resources, **Michael Gatari:** Resources. **Francis Pope:**
968 Supervision, Data curation, Funding acquisition, Writing - Review and Editing.

Deleted: ¶

970 **Acknowledgements:**

971 The work is funded by the UK Department for International Development (DFID) via the EPSRC grant 'Digital
972 Air Quality' (EP/T030100/1) and by the East Africa Research Fund (EARF) grant 'A Systems Approach to Air
973 Pollution (ASAP) East Africa'. The practical support of the Schools of Geography and Earth Sciences and
974 Engineering at the University of Birmingham are gratefully acknowledged.

975

976 **Data Availability:** the combined DICE-EDGAR anthropogenic emission inventory is downloadable from:

977 <https://doi.org/10.25500/edata.bham.00000695>

978

979 **References**

- 980 Alduchov O., E. R.: Improved Magnus Form Approximation of Saturation Vapor Pressure, *J. Of Appl.*
981 *Met.*, 35, 601-609, [https://doi.org/10.1175/1520-0450\(1996\)035<0601:IMFAOS>2.0.CO;2](https://doi.org/10.1175/1520-0450(1996)035<0601:IMFAOS>2.0.CO;2), 1996.
- 982 Amegah, A. K., and Agyei-Mensah, S.: Urban air pollution in Sub-Saharan Africa: Time for action,
983 *Environ Pollut*, 220, 738-743, [10.1016/j.envpol.2016.09.042](https://doi.org/10.1016/j.envpol.2016.09.042), 2017.
- 984 Anav, A., Menut, L., Khvorostyanov, D., and VIOvy, N.: Impact of tropospheric ozone on the Euro-
985 Mediterranean vegetation, *Global Change Biology*, 17, 2342-2359, [10.1111/j.1365-](https://doi.org/10.1111/j.1365-2486.2010.02387.x)
986 [2486.2010.02387.x](https://doi.org/10.1111/j.1365-2486.2010.02387.x), 2011.
- 987 Assamoi, E.-M., and Liousse, C.: A new inventory for two-wheel vehicle emissions in West Africa for
988 2002, *Atmospheric Environment*, 44, 3985-3996, [10.1016/j.atmosenv.2010.06.048](https://doi.org/10.1016/j.atmosenv.2010.06.048), 2010.
- 989 Avis W. and Khaemba W.: Vulnerability and air pollution, 2018.
- 990 Barnard, J.: An evaluation of the FAST-J photolysis algorithm for predicting nitrogen dioxide
991 photolysis rates under clear and cloudy sky conditions, *Atmospheric Environment*, 38, 3393-3403,
992 [10.1016/j.atmosenv.2004.03.034](https://doi.org/10.1016/j.atmosenv.2004.03.034), 2004.
- 993 Bessagnet, B., Pirovano, G., Mircea, M., Cuvelier, C., Aulinger, A., Calori, G., Ciarelli, G., Manders, A.,
994 Stern, R., Tsyro, S., García Vivanco, M., Thunis, P., Pay, M.-T., Colette, A., Couvidat, F., Meleux, F.,
995 Rouil, L., Ung, A., Aksoyoglu, S., Baldasano, J. M., Bieser, J., Briganti, G., Cappelletti, A., D'Isidoro, M.,
996 Finardi, S., Kranenburg, R., Silibello, C., Carnevale, C., Aas, W., Dupont, J.-C., Fagerli, H., Gonzalez, L.,
997 Menut, L., Prévôt, A. S. H., Roberts, P., and White, L.: Presentation of the EURODELTA III
998 intercomparison exercise – evaluation of
999 the chemistry transport models' performance on criteria pollutants and joint
1000 analysis with meteorology, *Atmospheric Chemistry and Physics*, 16, 12667-12701, [10.5194/acp-16-](https://doi.org/10.5194/acp-16-12667-2016)
1001 [12667-2016](https://doi.org/10.5194/acp-16-12667-2016), 2016.
- 1002 Bian, H., Prather, M.: Fast-J2: accurate simulation of stratospheric photolysis in global chemical
1003 models, *J. Atmos. Chem*, 41, 281–296, <https://doi.org/10.1023/A:1014980619462>, 2002.
- 1004 Bockarie, A. S., Marais, E. A., and MacKenzie, A. R.: Air Pollution and Climate Forcing of the Charcoal
1005 Industry in Africa, *Environ Sci Technol*, 54, 13429-13438, [10.1021/acs.est.0c03754](https://doi.org/10.1021/acs.est.0c03754), 2020.
- 1006 Boylan, J. W., and Russell, A. G.: PM and light extinction model performance metrics, goals, and
1007 criteria for three-dimensional air quality models, *Atmospheric Environment*, 40, 4946-4959,
1008 [10.1016/j.atmosenv.2005.09.087](https://doi.org/10.1016/j.atmosenv.2005.09.087), 2006.

1010 Brauer, M., Amann, M., Burnett, R. T., Cohen, A., Dentener, F., Ezzati, M., Henderson, S. B.,
1011 Krzyzanowski, M., Martin, R. V., Van Dingenen, R., van Donkelaar, A., and Thurston, G. D.: Exposure
1012 assessment for estimation of the global burden of disease attributable to outdoor air pollution,
1013 Environ Sci Technol, 46, 652-660, 10.1021/es2025752, 2012.
1014 Carter, W. P. L.: Development of the SAPRC-07 chemical mechanism, Atmospheric Environment, 44,
1015 5324-5335, 10.1016/j.atmosenv.2010.01.026, 2010.
1016 Collins, W., Rasch, P., Boville, B., Hack, J., McCaa, J., Williamson, D., Kiehl, J., Briegleb, B., :
1017 Description of the NCAR Community Atmosphere Model (CAM 3.0). , NCAR Tech Notes, 2004.
1018 Crippa M., G. D., Muntean M., Shaaf E., Dentener F., van Aardenne J.A., Monni S., Doering U., Olivier
1019 J.G.J., Pagliari V. and Janssens-Maenhout G.: Gridded emissions of air pollutants for the period 1970-
1020 2012 within EDGAR v4.3.2, Earth Sci. Data, 10, 1987 – 2013, <https://doi.org/10.5194/essd-2018-31>,
1021 2018.
1022 Dalal, S., Beunza, J. J., Volmink, J., Adebamowo, C., Bajunirwe, F., Njelekela, M., Mozaffarian, D.,
1023 Fawzi, W., Willett, W., Adami, H. O., and Holmes, M. D.: Non-communicable diseases in sub-Saharan
1024 Africa: what we know now, Int J Epidemiol, 40, 885-901, 10.1093/ije/dyr050, 2011.
1025 deSouza P., N. V., Klopp J. M., Shaw B. E., Ho W. O., Saffell J., Jones R. and Ratti C.: : A Nairobi
1026 experiment in using low cost air quality monitors, Clean Air Journal, 27, 12-42,
1027 <http://dx.doi.org/10.17159/2410-972X/2017/v27n2a6>, 2017.
1028 Egondi, T., Kyobutungi, C., Ng, N., Muindi, K., Oti, S., van de Vijver, S., Ettarh, R., and Rocklöv, J.:
1029 Community perceptions of air pollution and related health risks in Nairobi slums, Int J Environ Res
1030 Public Health, 10, 4851-4868, 10.3390/ijerph10104851, 2013.
1031 Guidance for regulatory application of the urban airshed model UAM, 1991.
1032 Revised Air Quality Standards for particle pollution and updates to the Air Quality Index (AQI):
1033 https://www.epa.gov/sites/production0-etrfgvgy8ufiles/2016-04/documents/2012_aqi_factsheet.pdf
1034 2012.
1035 Gaita, S. M., Boman, J., Gatari, M. J., Pettersson, J. B. C., and Janhäll, S.: Source apportionment and
1036 seasonal variation of PM_{2.5} in a Sub-Saharan African city: Nairobi, Kenya, Atmospheric
1037 Chemistry and Physics, 14, 9977-9991, 10.5194/acp-14-9977-2014, 2014.
1038 Gatari, M. J., Kinney, P. L., Yan, B., Sclar, E., Volavka-Close, N., Ngo, N. S., Mwaniki Gaita, S., Law, A.,
1039 Ndiba, P. K., Gachanja, A., Graeff, J., and Chillrud, S. N.: High airborne black carbon concentrations
1040 measured near roadways in Nairobi, Kenya, Transportation Research Part D: Transport and
1041 Environment, 68, 99-109, 10.1016/j.trd.2017.10.002, 2019.
1042 Guenther, A., Karl, T., Harley, P., Wiedinmyer, C., Palmer, P., and Geron, C.: : Estimates of global
1043 terrestrial isoprene emissions using MEGAN (Model of Emissions of Gases and Aerosols from
1044 Nature), Atmos. Chem. Phys, 6, 3181–3210, <https://hal.archives-ouvertes.fr/hal-00295995>, 2006.
1045 Hauglustaine, D. A., Hourdin, F., Jourdain, L., Filiberti, M. A., Walters, S., Lamarque, J. F., and Holland,
1046 E. A.: Interactive chemistry in the Laboratoire de Météorologie Dynamique general circulation
1047 model: Description and background tropospheric chemistry evaluation, Journal of Geophysical
1048 Research: Atmospheres, 109, n/a-n/a, 10.1029/2003jd003957, 2004.
1049 Haywood, J. M., Pelon, J., Formenti, P., Bharmal, N., Brooks, M., Capes, G., Chazette, P., Chou, C.,
1050 Christopher, S., Coe, H., Cuesta, J., Derimian, Y., Desboeufs, K., Greed, G., Harrison, M., Heese, B.,
1051 Highwood, E. J., Johnson, B., Mallet, M., Marticorena, B., Marsham, J., Milton, S., Myhre, G.,
1052 Osborne, S. R., Parker, D. J., Rajot, J. L., Schulz, M., Slingo, A., Tanré, D., and Tulet, P.: Overview of
1053 the Dust and Biomass-burning Experiment and African Monsoon Multidisciplinary Analysis Special
1054 Observing Period-0, Journal of Geophysical Research, 113, 10.1029/2008jd010077, 2008.
1055 Hong S., D. J., and Shu–Hua Chen S.: A revised approach to ice microphysical processes for the bulk
1056 parameterization of clouds and precipitation, Mon. Wea. Rev, 132, 103-120,
1057 [https://journals.ametsoc.org/view/journals/mwre/132/1/1520-](https://journals.ametsoc.org/view/journals/mwre/132/1/1520-0493_2004_132_0103_aratim_2.0.co_2.xml)
1058 [0493_2004_132_0103_aratim_2.0.co_2.xml](https://journals.ametsoc.org/view/journals/mwre/132/1/1520-0493_2004_132_0103_aratim_2.0.co_2.xml), 2004.

1059 Hong S., N. Y., Dudhia J.: A new vertical diffusion package with an explicit treatment of entrainment
1060 processes, *Mon. Wea. Rev.*, 134, 2318–2341,
1061 <https://journals.ametsoc.org/view/journals/mwre/134/9/mwr3199.1.xml>, 2006.

1062 Kerandi, N., Arnault, J., Laux, P., Wagner, S., Kitheka, J., and Kunstmann, H.: Joint atmospheric-
1063 terrestrial water balances for East Africa: a WRF-Hydro case study for the upper Tana River basin,
1064 *Theoretical and Applied Climatology*, 131, 1337-1355, 10.1007/s00704-017-2050-8, 2017.

1065 Kerandi, N. M., Laux, P., Arnault, J., and Kunstmann, H.: Performance of the WRF model to simulate
1066 the seasonal and interannual variability of hydrometeorological variables in East Africa: a case study
1067 for the Tana River basin in Kenya, *Theoretical and Applied Climatology*, 130, 401-418,
1068 10.1007/s00704-016-1890-y, 2016.

1069 Kinney, P. L., Gichuru, M. G., Volavka-Close, N., Ngo, N., Ndiba, P. K., Law, A., Gachanja, A., Gaita, S.
1070 M., Chillrud, S. N., and Sclar, E.: Traffic Impacts on PM(2.5) Air Quality in Nairobi, Kenya, *Environ Sci*
1071 *Policy*, 14, 369-378, 10.1016/j.envsci.2011.02.005, 2011.

1072 Kume, A., Charles, K., Berehane, Y., Anders, E. and Ali, A.: Magnitude and variation of traffic air
1073 pollution as measured by CO in the City of Addis Ababa, Ethiopia, *Ethiopian Journal of Health*
1074 *Development*, 24, <https://doi.org/10.4314/ejhd.v24i3.68379>, 2010.

1075 Lacaux, J. P., Brustet, J.M., Delmas, R. et al.: Biomass burning in the tropical savannas of Ivory Coast:
1076 An overview of the field experiment Fire of Savannas (FOS/DECAFE 91), *J Atmos Chem*, 22, 195–216,
1077 <https://doi.org/10.1007/BF00708189>, 1995.

1078 Li, C., Martin, R. V., van Donkelaar, A., Boys, B. L., Hammer, M. S., Xu, J. W., Marais, E. A., Reff, A.,
1079 Strum, M., Ridley, D. A., Crippa, M., Brauer, M., and Zhang, Q.: Trends in Chemical Composition of
1080 Global and Regional Population-Weighted Fine Particulate Matter Estimated for 25 Years, *Environ Sci*
1081 *Technol*, 51, 11185-11195, 10.1021/acs.est.7b02530, 2017.

1082 Liousse, C., Guillaume, B., Grégoire, J. M., Mallet, M., Galy, C., Pont, V., Akpo, A., Bedou, M., Castéra,
1083 P., Dungall, L., Gardrat, E., Granier, C., Konaré, A., Malavelle, F., Mariscal, A., Mieville, A., Rosset, R.,
1084 Serça, D., Solmon, F., Tummon, F., Assamoi, E., Yoboué, V., and Van Velthoven, P.: Updated African
1085 biomass burning emission inventories in the framework of the AMMA-IDAF program, with an
1086 evaluation of combustion aerosols, *Atmospheric Chemistry and Physics*, 10, 9631-9646,
1087 10.5194/acp-10-9631-2010, 2010.

1088 Liousse, C., Assamoi, E., Criqui, P., Granier, C., & Rosset, R.: Explosive growth in African combustion
1089 emissions from 2005 to 2030, *Environmental Research Letters*, 9, [https://doi.org/10.1088/1748-](https://doi.org/10.1088/1748-9326/9/3/035003)
1090 [9326/9/3/035003](https://doi.org/10.1088/1748-9326/9/3/035003), 2014.

1091 Loosmore, G. A., and Cederwall, R. T.: Precipitation scavenging of atmospheric aerosols for
1092 emergency response applications: testing an updated model with new real-time data, *Atmospheric*
1093 *Environment*, 38, 993-1003, <https://doi.org/10.1016/j.atmosenv.2003.10.055>, 2004.

1094 Mailler, S., Menut, L., Khvorostyanov, D., Valari, M., Couvidat, F., Siour, G., Turquety, S., Briant, R.,
1095 Tuccella, P., Bessagnet, B., Colette, A., Létinois, L., Markakis, K., and Meleux, F.: CHIMERE-2017: from
1096 urban to hemispheric chemistry-transport modeling, *Geoscientific Model Development*, 10, 2397-
1097 2423, 10.5194/gmd-10-2397-2017, 2017.

1098 Marais, E. A., and Wiedinmyer, C.: Air Quality Impact of Diffuse and Inefficient Combustion Emissions
1099 in Africa (DICE-Africa), *Environ Sci Technol*, 50, 10739-10745, 10.1021/acs.est.6b02602, 2016.

1100 Marais, E. A., Silvern, R. F., Vodonos, A., Dupin, E., Bockarie, A. S., Mickley, L. J., and Schwartz, J.: Air
1101 Quality and Health Impact of Future Fossil Fuel Use for Electricity Generation and Transport in Africa,
1102 *Environ Sci Technol*, 53, 13524-13534, 10.1021/acs.est.9b04958, 2019.

1103 Markakis, K., Valari, M., Perrussel, O., Sanchez, O., and Honore, C.: Climate-forced air-quality
1104 modeling at the urban scale: sensitivity to model resolution, emissions and meteorology,
1105 *Atmospheric Chemistry and Physics*, 15, 7703-7723, 10.5194/acp-15-7703-2015, 2015.

1106 Mazzeo, A., Huneeus, N., Ordoñez, C., Orfanos-Chequela, A., Menut, L., Mailler, S., Valari, M., van
1107 der Gon, H. D., Gallardo, L., and Muñoz, R.: Impact of residential combustion and transport
1108 emissions on air pollution in Santiago during winter, *Atmospheric Environment*, 190, 195-208, 2018.

1109 Mbewu, A., Mbanya, J.C., : Disease and Mortality in Sub-Saharan Africa, in: Cardiovascular disease
1110 edited by: Bank, W., 2006.

1111 Nenes, A., Pilinis, C., Pandis, S.: : Isorropia: a new thermodynamic model for inorganic
1112 multicomponent atmospheric aerosols., *Aquat. Geochem*, 4, 123-152,
1113 <https://doi.org/10.1023/A:1009604003981>, 1998.

1114 Ngo, N. S., Gatari, M., Yan, B., Chillrud, S. N., Bouhamam, K., and Kinney, P. L.: Occupational
1115 exposure to roadway emissions and inside informal settlements in sub-Saharan Africa: A pilot study
1116 in Nairobi, Kenya, *Atmos Environ* (1994), 111, 179-184, 10.1016/j.atmosenv.2015.04.008, 2015.

1117 Ogega O.M., W. H. N., Mbugua J: Exploring the Future of Nairobi National Park in a Changing Climate
1118 and Urban Growth., in: *The Geography of Climate Change Adaptation in Urban Africa.*, edited by:
1119 Macmillan, P., 2019.
1120 [https://open.africa/dataset/kenya-administrative-boundaries/resource/b5bee56d-b7cb-4f23-8f2b-](https://open.africa/dataset/kenya-administrative-boundaries/resource/b5bee56d-b7cb-4f23-8f2b-356ca0044bf3)
1121 [356ca0044bf3](https://open.africa/dataset/kenya-administrative-boundaries/resource/b5bee56d-b7cb-4f23-8f2b-356ca0044bf3), 2018.

1122 Pai, S. J., Heald, C. L., Pierce, J. R., Farina, S. C., Marais, E. A., Jimenez, J. L., Campuzano-Jost, P., Nault,
1123 B. A., Middlebrook, A. M., Coe, H., Shilling, J. E., Bahreini, R., Dingle, J. H., and Vu, K.: An evaluation
1124 of global organic aerosol schemes using airborne observations, *Atmospheric Chemistry and Physics*,
1125 20, 2637-2665, 10.5194/acp-20-2637-2020, 2020.

1126 Parkin, D. M., Sitas, F., Chirenje, M., Stein, L., Abratt, R., and Wabinga, H.: Part I: Cancer in
1127 Indigenous Africans—burden, distribution, and trends, *The Lancet Oncology*, 9, 683-692,
1128 10.1016/s1470-2045(08)70175-x, 2008.

1129 Peña, M. a. R., A.: Environmental Exposures and Cardiovascular Disease, *Cardiology clinics*, 35, 71-86,
1130 <https://doi.org/10.1016/j.ccl.2016.09.001>, 2017.

1131 Petkova, E. P., Jack, D. W., Volavka-Close, N. H., and Kinney, P. L.: Particulate matter pollution in
1132 African cities, *Air Quality, Atmosphere and Health*, 6, 603-614, [https://doi.org/10.1007/s11869-013-](https://doi.org/10.1007/s11869-013-0199-6)
1133 [0199-6](https://doi.org/10.1007/s11869-013-0199-6), 2013.

1134 Pohl, B., Créta, J., and Camberlin, P.: Testing WRF capability in simulating the atmospheric water
1135 cycle over Equatorial East Africa, *Climate Dynamics*, 37, 1357-1379, 10.1007/s00382-011-1024-2,
1136 2011.

1137 Pope, F. D., Gatari, M., Ng'ang'a, D., Poynter, A., and Blake, R.: Airborne particulate matter
1138 monitoring in Kenya using calibrated low-cost sensors, *Atmospheric Chemistry and Physics*, 18,
1139 15403-15418, 10.5194/acp-18-15403-2018, 2018.

1140 Powers, J. G., Klemp, J.B., Skamarock, W.C., Davis, C.A., Dudhia, J., Gill, D.O., Coen, J.L., Gochis, D.J.,
1141 Ah madov, R., Peckham, S.E., Grell, G.A., Michalakes, J., Trahan, S., Benjamin, S.G., Alexander, C.R.,
1142 Di mego, G.J., Wang, W., Schwartz, C.S., Romine, G.S., Liu, Z., Snyder, C., Chen, F., Barlage, M.J., Yu,
1143 W., Duda, M.G.: : The weather research and forecasting model: overview, system efforts, and future
1144 directions, *Bull. Am. Meteorol. Soc.*, 98, 1717–1737, <https://doi.org/10.1175/BAMS-D-15-00308.1>,
1145 2017.

1146 Pun, B. K., Seigneur, C., and Lohman, K.: Modeling secondary organic aerosol formation via
1147 multiphase partitioning with molecular data, *Environ. Sci. Technol.*, 40, 4722–4731,
1148 <https://doi.org/10.1021/es0522736>, 2006.

1149 Real, E., and Sarlet, K.: Modeling of photolysis rates over Europe: impact on chemical gaseous
1150 species and aerosols, *Atmospheric Chemistry and Physics*, 11, 1711-1727, 10.5194/acp-11-1711-
1151 2011, 2011.

1152 Schwander, S., Okello, C. D., Freers, J., Chow, J. C., Watson, J. G., Corry, M., and Meng, Q.: Ambient
1153 particulate matter air pollution in Mpererwe District, Kampala, Uganda: a pilot study, *J Environ*
1154 *Public Health*, 2014, 763934, 10.1155/2014/763934, 2014.

1155 Seinfeld, J. H., Pandis, S.N.: *Atmospheric chemistry and physics: from air pollution to climate change*,
1156 edited by: Sons, J. W., 2016.

1157 Singh, A., Avis, W. R., and Pope, F. D.: Visibility as a proxy for air quality in East Africa, *Environmental*
1158 *Research Letters*, 15, 10.1088/1748-9326/ab8b12, 2020.

1159 Singh, A., Ng'ang'a, D., Gatari, M., Kidane, A. W., Alemu, Z., Derrick, N., Webster, M. J., Bartington, S.,
1160 Thomas, N., Avis, W. R., and Pope, F.: Air quality assessment in three East African cities using
1161 calibrated low-cost sensors with a focus on road-based hotspots, *Environmental Research*
1162 *Communications*, 10.1088/2515-7620/ac0e0a, 2021.
1163 Skamarock, W., Klemp, J., Dudhia, J., Gill, D., Barker, D., Duda, M., Huang, X., Wang, W., Powers, J., :
1164 A description of the advanced research WRF version 3. NCAR, 2008.
1165 Teklay, A., Dile, Y. T., Asfaw, D. H., Bayabil, H. K., and Sisay, K.: Impacts of land surface model and
1166 land use data on WRF model simulations of rainfall and temperature over Lake Tana Basin, Ethiopia,
1167 *Heliyon*, 5, e02469, 10.1016/j.heliyon.2019.e02469, 2019.
1168 Telford, P. J., Abraham, N. L., Archibald, A. T., Braesicke, P., Dalvi, M., Morgenstern, O., O'Connor, F.
1169 M., Richards, N. A. D., and Pyle, J. A.: Implementation of the Fast-JX Photolysis scheme (v6.4) into the
1170 UKCA component of the MetUM chemistry-climate model (v7.3), *Geoscientific Model Development*,
1171 6, 161-177, 10.5194/gmd-6-161-2013, 2013.
1172 Tewari, M., F. Chen, W. Wang, J. Dudhia, M. A. LeMone, K. Mitchell, M. Ek, G. Gayno, J. Wegiel, and
1173 R. H. Cuenca.: Implementation and verification of the unified NOAA land surface model in the WRF
1174 model. In *Proceedings of the 20th Conference on Weather Analysis and Forecasting, 16th Conference*
1175 *on Numerical Weather Prediction*, Seattle, 2004.
1176 Thompson A. M., W. J. C., Hudson R. D., Guo H., Herman J. R., and Fujiwara M.: Tropical tropospheric
1177 ozone and biomass burning Science, 291, 2128-2132, 10.1126/science.291.5511.2128, 2001.
1178 Trewhela, B., Huneus, N., Munizaga, M., Mazzeo, A., Menut, L., Mailler, S., Valari, M., and Ordoñez,
1179 C.: Analysis of exposure to fine particulate matter using passive data from public transport,
1180 *Atmospheric Environment*, 215, 116878, 2019.
1181 UK, M. O.: Met Office Integrated Data Archive System (MIDAS) Land and Marine Surface Stations
1182 Data (1853-current). NCAS British Atmospheric Data Centre, date of citation. UK, M. O. (Ed.), 2012.
1183 New Urban Agenda <http://habitat3.org/wp-content/uploads/NUA-English.pdf>, 2017.
1184 City of Nairobi Environment Outlook: <https://wedocs.unep.org/handle/20.500.11822/8738>, 2009.
1185 FEWS NET: <https://fews.net/east-africa/seasonal-monitor/march-2022>, access: May 2022, 2022.
1186 Valari, M., and Menut, L.: Transferring the heterogeneity of surface emissions to variability in
1187 pollutant concentrations over urban areas through a chemistry-transport model, *Atmospheric*
1188 *Environment*, 44, 3229-3238, 10.1016/j.atmosenv.2010.06.001, 2010.
1189 Van Leer, B.: Towards the ultimate conservative difference scheme. V. A second-order sequel to
1190 Godunov's method. , *Journal of Computational Physics*, 32, 101–136, 10.1016/0021-9991(79)90145-
1191 1, 1979.
1192 van Loon, M., Vautard, R., Schaap, M., Bergström, R., Bessagnet, B., Brandt, J., Builtjes, P. J. H.,
1193 Christensen, J. H., Cuvelier, C., Graff, A., Jonson, J. E., Krol, M., Langner, J., Roberts, P., Rouil, L.,
1194 Stern, R., Tarrasón, L., Thunis, P., Vignati, E., White, L., and Wind, P.: Evaluation of long-term ozone
1195 simulations from seven regional air quality models and their ensemble, *Atmospheric Environment*,
1196 41, 2083-2097, 10.1016/j.atmosenv.2006.10.073, 2007.
1197 Vautard, R., Builtjes, P. H. J., Thunis, P., Cuvelier, C., Bedogni, M., Bessagnet, B., Honoré, C.,
1198 Moussiopoulos, N., Pirovano, G., and Schaap, M.: Evaluation and intercomparison of Ozone and
1199 PM10 simulations by several chemistry transport models over four European cities within the
1200 CityDelta project, *Atmospheric Environment*, 41, 173-188, 10.1016/j.atmosenv.2006.07.039, 2007.
1201 Vliet, V. E. a. K., P.: Impacts of roadway emissions on urban particulate matter concentrations in
1202 sub-Saharan Africa: new evidence from Nairobi, Kenya, *Environmental Scientific letters*, 2,
1203 <https://doi.org/10.1088/1748-9326/2/4/045028>, 2007.
1204 Voulgarakis, A., Savage, N. H., Wild, O., Carver, G. D., Clemitshaw, K. C., Pyle, J. A.: Upgrading
1205 photolysis in the PHOTOMCAT CTM: model evaluation and assessment of the role of clouds,
1206 *Geoscientific Model Development*, 2, 59-72, <https://doi.org/10.5194/gmd-2-59-2009>, 2009.
1207 World Bank Open Data: <https://data.worldbank.org/>, access: June 2022, 2022.
1208 WHO: WHO Air quality guidelines for particulate matter, ozone, nitrogen dioxide and sulfur dioxide,
1209 2005.

1210 WHO: Burden of disease from ambient air pollution for 2012, 2012.
1211 WHO: Ambient Air Pollution: A global assessment of exposure and burden of disease, 2016.
1212 Wild, O., Zhu, X., and Prather, J.: Fast-J: Accurate simulation of the in- and below cloud photolysis in
1213 tropospheric chemical models., *J. Atmos. Chem.*, 37, 245-282,
1214 <https://doi.org/10.1023/A:1006415919030>, 2000.
1215 Wu, W.-S., Purser, R.J., Parrish, D.F., : Three-dimensional variational analysis with spatially
1216 inhomogeneous covariances., *Mon. Weather Rev.*, 130, 2905–2916, [https://doi.org/10.1175/1520-0493\(2002\)130<2905:TDVAWS>2.0.CO;2](https://doi.org/10.1175/1520-0493(2002)130<2905:TDVAWS>2.0.CO;2), 2002.
1217 Zhang, L., Gong, S., Padro, J., and Barrie, L.: A size-segregated particle dry deposition scheme for an
1218 atmospheric aerosol module, *Atmospheric Environment*, 35, 549-560,
1219 [https://doi.org/10.1016/S1352-2310\(00\)00326-5](https://doi.org/10.1016/S1352-2310(00)00326-5), 2001.
1220 Zyryanov, D., Foret, G., Eremenko, M., Beekmann, M., Cammas, J. P., D'Isidoro, M., Elbern, H.,
1221 Flemming, J., Friese, E., Kioutsioutkis, I., Maurizi, A., Melas, D., Meleux, F., Menut, L., Moinat, P.,
1222 Peuch, V. H., Poupkou, A., Razinger, M., Schultz, M., Stein, O., Suttie, A. M., Valdebenito, A., Zerefos,
1223 C., Dufour, G., Bergametti, G., and Flaud, J. M.: 3-D evaluation of tropospheric ozone simulations by
1224 an ensemble of regional Chemistry Transport Model, *Atmospheric Chemistry and Physics*, 12, 3219-
1225 3240, 10.5194/acp-12-3219-2012, 2012.
1226
1227